



**SAPIENZA**  
UNIVERSITÀ DI ROMA

# **SAPIENZA UNIVERSITÀ DI ROMA**

DEPARTMENT OF MOLECULAR MEDICINE

IMMUNOLOGICAL HEMATOLOGICAL AND REUMATOLOGICAL SCIENCE

CURRICULUM: IMMUNOLOGY AND IMMUNOPATHOLOGY

## **Adoptive immunotherapy using PRAME-specific T cells in medulloblastoma**

Supervisor:

**Dr. Biagio De Angelis**

Co-supervisors:

**Prof. Concetta Quintarelli**

**PhD: Domenico Orlando**

Academic year 2018/19

# Index

<b>1.INTRODUCTION</b> .....	1
1.1. Medulloblastoma.....	1
1.2. Molecular characterization of MBsubgroups.....	2
1.3. MB Therapeutic approaches.....	5
1.4.Immunotherapy for MB .....	7
1.5.A new target for MB immunotherapy .....	13
<b>2.AIM OF WORK</b> .....	15
<b>3.MATERIALS AND METHODS</b> .....	16
3.1. Cell lines .....	16
3.2. Healthy Donor's PBMCs, MB patients and controls .....	16
3.3. Retroviral constructs .....	17
3.4. Generation and expansion of polyclonal iC9-SLL-TCR T cells .....	18
3.5. Activation of the suicide gene .....	18
3.6. Immunophenotyping .....	19
3.7. ELISpot assay.....	19
3.8.Co-Culture assays .....	19
3.9. IFN $\gamma$ ELISA .....	20
3.10. Chromium-release assay .....	20
3.11. RNA isolation and quantitative real time PCR.....	20
3.12. Molecular detection of retroviral transduced T cells.....	21
3.13. Xenograft mouse model for <i>in vivo</i> studies.....	21
3.14. Histological and immunohistochemistry data.....	22
3.15. Mouse Behavioural studies.....	23
3.16. Statistical analysis .....	23
<b>4.RESULTS</b> .....	25
4.1. PRAME expression in MB at diagnosis and relapse .....	25
4.2. Retroviral vector carrying iC9 and PRAME-SLL specific $\alpha\beta$ TCR allows stable and functional expression of the transgene .....	35

4.3. PRAME-specific TCR-redirected T cells exert antitumor activity toward HLA-A\*02-matched MB cell line ..... 41

4.4. iC9-SLL TCR T cells exert antitumor activity *in vivo* in xenogenic mouse model of MB..... 46

**5.DISCUSSION..... 51**

**REFERENCES..... 55**

# 1. Introduction

## 1.1. Medulloblastoma

Medulloblastoma (MB) is the most common malignant pediatric brain tumor. It represents about 15–20% of the central nervous system (CNS) malignancies, 40% of which are located in the posterior fossa.(1) Despite the evidence that survival rates have increased by 30% in the past 20 years, today many patients still have a poor prognosis. (2) MB are embryonic CNS tumors constituted by primitive-appearing cells that can differentiate along multiple lineages. It arise from cerebellum and it is not completely understood which specific cells subset gives rise to these malignancies. One common theory is that MB starts from mutations in proliferating granule neuron precursors (GNPs) in the external germinal/granular layer (EGL). (3) The histological disease features reveal a heterogeneous disorder, in fact four variants of MB have been identified: classic, desmoplastic/nodular (D/N), extensive nodularity (MBEN), anaplastic and large cell, the latter often coexisting in the large cell/anaplastic (LC/A) variant. (4,5) MB is not a single disease, but a heterogeneous mixture of various subgroups with distinct features. The genomic profiles show four distinct molecular subgroups that have been identified: Wingless (WNT), Sonic Hedgehog (SHH), Group 3 and Group 4. (6,7)(Figure 1) Each subgroup corresponds to specific survival rate, age demographics, and genetic aberrations.(8) WNT and SHH subgroups are named after the discovery of the signaling pathway that plays a prominent role in the pathogenesis. (9) Molecular subgroups are correlated to clinical outcome. For this reason, they were integrated in the most recent version of WHO classification of CNS malignancies (5) and applied into the clinical practice. These MB subgroups remain stable at recurrence and are likely remindful of original cells. Recent research on 763 MB samples by Cavalli and colleagues (10) has shown the presence of inter-tumoral heterogeneity within the four MB subgroups delineating the presence of 12 subtypes based on gene expression and DNA methylation features, but the degree of heterogeneity and the extent of overlap are still unknown. This newfound heterogeneity within subgroups could explain previously unknown variation.(10) Thus, much emphasis has been recently placed on further identifying new alterations that may occur in each subtype pathway. Moreover, Northcott et al. described the



whole genome landscape of MB subtypes analysing 491 patient tumours.(11) They showed that driver mutations could be assigned to the two most malignant forms, group 3 and group 4 MB. In particular, in-frame insertions hotspot that target KBTBD4 (Kelch Repeat And BTB Domain Containing 4) and activation of PR/SET Domain 6 (PRDM6) were identified.(11) These and other novel findings identified in the MB subgroups could lead to the discovery of attractive targets for MB, which have not previously been explored in detail.

## **1.2. Molecular characterization of MB subgroups**

WNT is the less common molecular MB subgroup and accounts for about 10– 11% of all MB. (12) It shows the main incidence at 10–12 years of age, being very rare in infants, with no differences in gender predilection. The typical histology is most frequently encountered, with rare cases of the LC/A variant and metastatic dissemination. (13) The main characteristic in WNT tumors is the somatic activating mutations in exon 3 of  $\beta$ -catenin (CTNNB1), shown in 85% of WNT MB with a predictive good outcome for patients. (14) However, the link between a better prognosis due to biological effect of Wnt/ $\beta$ -catenin signaling activation have not been fully clarified yet. (15) Monosomy 6 is the primary recurrent structural chromosomic alteration, present in the 80–85% of cases. Other common mutations are in DDX3X gene and the missense mutations in TP53 (15% of cases), that is a marker of high risk in the SHH subgroup but with no evidence in differences in the WNT patients survival rate. (16)






The SHH subgroup that represents 28–30% of all MB, has a bimodal age distribution, being more frequent in infants and adults, with a weak male predominance among infants. (17) The prognosis depends on the associated mutation meaning that these patients have an intermediate prognosis, with 5-years survival ranging between 60% and 80%, but the mutations in MYCN or TP53 oncogenes worsen the prognosis. (18) D/N and MBEN histology are the main features associated with the SHH subtype, however, it is also possible to observe classic or LC/A histology. (13) There are typical genetic alterations that lead to the SHH signaling over-activation: the most common ones are the somatic or germ-line inactivating alterations or the loss of

PTCH1 and SUFU, or the somatic missense mutations activating SMO. (19,20) Few SHH patients showed high-risk disease due to co-amplification of MYCN and GLI2, accompanied by inactivation of TP53. (16) Patients with Gorlin syndrome, carriers of a germ-line mutation on PTCH1, have a predisposition to develop basal-cell carcinoma and MB, especially MBEN. (21) Unusual SHH subgroup MBs has also been reported in patients with rare diseases such as Fanconi anemia. (22)

The Group 3 has around 25-28% incidence of all MB and these patients exhibit the worst survival rate and the highest rate of metastatic dissemination. (23) Group 3 MBs are very rare in adults but are common in infants and younger children, with a male to female ratio of 2:1. (13) LC/A is the principal histology and the tumor genome is considerably unbalanced. Several numbers of broad alterations were find such as gain of chromosome 7 and iso-chromosome 17q. There are also associations with neurocutaneous syndromes such as tuberous sclerosis complex that have been described. (24)

Group 4 MBs share many of these alterations.(25) The most common event is the MYC amplification (10– 20%), followed by OTX2 transcription factor mutations, which affect the 10% of patients and is mutually exclusive of MYC amplification. The incidence of Group 4 is about 34–35% of all MBs, and it is the most common subgroup. (12)This subgroup is rare in infants, it exhibit a peak incidence in 10-years-old children, with a prevalence in males (sex ratio 3:1). They can have classic or LC/A histology. Group 4 MBs have an intermediate prognosis and show a high rate of metastasis and relapse. MYCN amplification is not associated with the worst outcome such as the SHH subgroup. (26)

**Figure 1**

	WNT	SHH	Group 3	Group 4
Age group 				
Gender ratio (♂:♀)	1 : 1	1 : 1	2 : 1	3 : 1
Outcome	Very good	Infants good, others intermediate	Poor	Intermediate
Anatomic location	Brainstem, 4th ventricle	Cerebellar hemispheres	Midline, 4th ventricle	Midline, 4th ventricle
Metastasis at diagnosis	5-10%	15-20%	40-45%	35-40%
Pattern of recurrence	Rare. Can be local or metastatic	Local	Metastatic	Metastatic
Genetic alterations	<i>CTNNB1</i> , <i>DDX3X</i> , <i>SMARCA4</i> , <i>TP53</i> mutation	<i>PTCH1</i> , <i>SMO</i> , <i>SUFU</i> , <i>TP53</i> mutation <i>GLI2</i> , <i>MYCN</i> amplification	<i>GLI1</i> , <i>GFL1B</i> activation, <i>MYC</i> , <i>OTX-2</i> amplification, <i>SMARCA4</i> mutation	<i>KDM6A</i> mutation, <i>SNCAIP</i> duplication <i>CDK6</i> , <i>MYCN</i> amplification
Cytogenetic aberrations	Monosomy 6	3q gain 9q, 10q, 17p loss	i17q 1q, 7, 18 gain 10q, 11, 16q, 17p loss	i17q 7q, 18q gain 8p, 11p, X loss

**Figure 1. Molecular subgroups of medulloblastoma.** WNT: wingless, SHH: sonic hedgehog, M : male, F : female. (27)

### **1.3. MB therapeutic approaches**

Nowadays the treatment for MB is based on surgery followed by craniospinal chemotherapy and irradiation. However, CNS radiation therapy can be harmful to the developing brain and is usually spared in children under the age of three, but this can affect the disease control and survival. Moreover, the post-surgery treatment with chemotherapy and irradiation are fundamental to eliminate any residual tumor cells leading to the reduction of metastases risk occurrence. However, it is relevant to consider that the same treatments leading to increased survival rates are also causing potentially debilitating physical deficits, such as endocrine dysfunction, neuropsychological deficits or subsequent malignancies. Indeed, the outcomes in 51 long-term survivors of paediatric MB were comprehensively assessed in terms of tumour control, neurological, endocrine, and neurocognitive complications and their impact on behavioural and psychological adjustment, and health-related quality of life (QoL). (28) Endocrine deficits occurred in 61%, neurological complications in 72%, and significant school problems in 72%. All patients had significant deficits in neurocognitive functioning: attention and processing speed was impaired in 79%, learning and memory in 88%, language in 56%, visual perception in 50%, and executive functions in 64%. Because of their treatment, including craniospinal radiotherapy, MB long-time survivors are not only at great risk for neurological, endocrine, and neurocognitive complications, but also of social isolation thereby decreasing self-rated QoL substantially.

Thus, there is a need for the development of new strategies that may significantly ameliorate outcome and QoL especially in the younger population and decrease potential side effects. MB tumors possess peculiar features different from peripheral tumors, and many factors such as the blood brain barrier (BBB) and the hostile tumor microenvironment should be considered. The disease understanding is critical, in fact one of the major obstacles is the drug delivery due to the MB brain localization. The tumor cells usually grow in the cerebellum midline. The patients present increased intracranial pressure (ICP) and typical signs of obstructive hydrocephalus. The symptoms usually are headaches and nausea/vomiting for weeks to months prior to disease discovery. Irritability and poor feeding could also affect young children, with severe cases that show altered mental status. Other physical signs found during patients' examination are bradycardia, hypertension and widened pulse pressure.

With a severe hydrocephalous degree we can have ocular findings such as papilledema and 6th nerve palsies.(29) The perfect scenery for MB patients is the maximal tumor resection and the first step is the surgery. Approximately 25% of MB patients develop the posterior fossa syndrome after surgery, leading to some degree of cerebellar mutism where patients try to produce words but are unable and start to be extremely irritable, and provoke hypotonia and ataxia. The syndrome is usually exhibited 24 hours after resection of a posterior fossa tumor and the duration is variable from weeks to months, but the language difficulties may be lifelong.(30) Other complications of surgery include disruption of the blood supply leading to infarction of surrounding normal brain, and intra-operative bleeding leading to subdural hematomas. 30 days after definitive surgery the patients is recruited for the radiation therapy (XRT).(31,32) Daily fractions of 1.8 Gy to a final dose of 54 Gy - 59.4 Gy are used. There is high risk to develop complications due to XRT for pediatric patients with MB. Radiation therapy could lead to anorexia and nausea due to the proximity of the spinal fields to the gastro intestinal tract. It is fundamental to control the patient's weight and nutrition during the treatment. The bone marrow of the vertebral bodies is active and important for the maintenance of normal blood counts, so cytopenias often appear during this period. Most MB patients require XRT for long term survival, and treatment costs are very expensive.

Moreover, another approach is the pharmacological treatment. It is based on chemotherapy drugs administration and the aim is to enhance the local control of tumor and the management of micrometastatic disease. The drugs' mechanism affects rapidly dividing cells and also damages the gastro intestinal tract, hair follicles, and bone marrow. This leads to risk of nausea and vomiting, diarrhea and/or constipation, hair loss and myelosuppression. The chemotherapy is used specifically depending on the MB patient characteristic and there are protocols to well establish the correct treatment. Some examples of used drugs are: Cisplatin, mechanism of action: induces cellular apoptosis by cross-linking DNA;(33) Cyclophosphamide, mechanism of action: alkylating agent; Lomustine, mechanism of action: alkylating agent; Vincristine, mechanism of action: microtubule inhibitor that prevents cell division by binding to the tubulin component of microtubules and leading to metaphase arrest.(34)

## 1.4. Immunotherapy for MB

Cancer immunotherapy is a new advanced medicine approach that allows triggering the cytotoxic potential of the immune system against cancer cells. In particular, T cells adoptive immunotherapy is one of the best-characterized and used strategies nowadays, with several clinical trials opened worldwide. T cells are the cells responsible to fight foreign pathogens that pretend to be 'self'. T cells are able to recognize mutated or infected cells through antigens (small peptides) presented by the major histocompatibility complex (MHC) class. (35) Tumor cells evolve through mutations from the phenotype of their origin cells and de-differentiate and up-regulate the expression of proteins normally not exhibited by the origin cells, the tumor associated antigens (TAA). Cancer immunotherapy is based on the possibility of T cells (or other immune system component) to recognize TAA. Unlike traditional pharmacologic agents that require increased titration for full effect (often with dose limiting toxicities that preclude rampant dose escalation), immunotherapy is a biologic agent that may not necessitate the same dose-dependent increases for maximal impact. (36) For instance, the law of the impassable BBB is now changing opening new scenery for the in "vivo biology" respect the difficulties of the bio-distribution of pharmacological treatment. Recently, lymphatic drainage networks have been described within the CNS that communicate with deep cervical draining lymph nodes. (37-41) Activated T cells able to recognize tumor-specific antigens are able to traverse the BBB through adhesion markers (i.e., VLA-4), allowing them to penetrate the tumor microenvironment and induce their effector functions against pediatric cancer cells. (37-41)

For children with malignant brain tumors, immunotherapy may be used in conjunction with standard therapy but we should consider the impact of traditional protocols on the immunotherapy treatment. XRT may confound Th1 type responses by decreasing CD8+ dendritic cells (42,43) but can damage the tumor environment with the release of damage associated molecular patterns (DAMPs) and tumor antigens that can be processed by endogenous antigen presenting cells (APCs) for presentation to T cells in local draining lymph nodes. (44) Instead, chemotherapy can be directly toxic to activated T cells, but may eliminate regulatory populations (i.e., regulatory T cells, myeloid derived suppressor cells) that compete for essential cytokines. (45-47) The adoptive cellular therapy is best utilized after radiation and chemotherapy; moreover,

all these treatment modalities may synergize also with a vaccine immunotherapy. (48,49) Preclinical and clinical investigations have shown that vaccination through repeated cycles of chemotherapy enhances antigen specific T cell immunity.(49–51) We can image to use an adoptive cellular therapy followed after by chemotherapy with continued vaccination cycles to maintain immunologic memory.

Focusing our attention on pediatric brain tumors, appropriate tumor antigens have to be selected and targeted, avoiding immunologic targeting of epitopes expressed on normal tissue that may elicit autoimmunity. (52) Most pediatric brain tumors have low mutational rate at the genomic level but are prompted by epigenetic deregulatory mechanisms that lead to the re-expression of developmental fetal antigens in malignancies, such as MB and primitive neural ectodermal tumors (PNETs). (53-55)

The immune system actively survey against cancer and is able to recognize and remove cells that are undergoing oncologic transformation.(56,57)The immune system triggers a response when a critical mass of cancer cells develops, but consequently, tumor cells evolve to escape the immune surveillance and re-populate the mass.(56,57) (Figure2) This new tumor microenvironment becomes comprised of immunoregulatory populations, including FoxP3+ regulatory T cells, tumor associated macrophages, and myeloid derived suppressor cells, which actively suppress the cytotoxic effect modulating effector T cells.(58–60) Immunotherapy can be employed to help the cytotoxic components to escape the hostile tumor environment in order to develop a novel effective tumor response.

Immune checkpoint blockade antagonizes inhibitory receptor/ligand interactions (i.e., programmed death-ligand 1 (PD-L1) on APCs and tumor cells/programmed death-1 (PD-1) receptor on T cells) designed to inhibit activated T cells.(61)Today with monoclonal antibodies (mAbs) we are able to block these inhibitory axes in order to re-activate T cells and to elicit their anti-tumor effector functions.(61) Checkpoint inhibitors have been shown remarkable results against adult cancers (i.e., skin and lung), but pediatric malignancies are distinct.(62) Moreover, immune checkpoint mAbs are not expected to cross the BBB; however, in the presence of tumor, chemotherapy and radiation, this barrier may be perturbed, allowing these molecules to translocate. (63,64) Clinical trials are currently underway in children with high grade gliomas (HGGs) and DIPGs (phase I, [clinicaltrials.gov: NCT02359565](https://clinicaltrials.gov/ct2/show/study/NCT02359565)) to

determine the utility of these agents against pediatric CNS malignancies.

Since childhood brain cancer is a developmental topic, the generation of novel immunotherapy strategies is necessary. While checkpoint inhibitors (i.e., PD-1 and PD-L1 mAbs) are promising candidates that can be leveraged for all patients, they appear to require tumors with high mutational burdens and PD-1+ intratumoral T cells (or high expressing PD-L1+ tumors).(61,62) CD47 is an immune evasion marker on the surface of many solid cancers that could be used as a tumor immunosuppressive target. (65) CD47 is overexpressed by malignant cells to evade the innate immune response and may be particularly enriched in pediatric brain tumors including MB, acute teratoid rhabdoid tumor, pediatric glioblastoma, and DIPG.(65) Pre-clinical studies with a humanized mAbs antagonizing CD47 have demonstrated that macrophages can be unlocked to phagocytize tumor cells in several pediatric brain tumor models. (65) In addition to CD47 targeting, tumor immunosuppression can be overcome through targeting indoleamine 2,3-dioxygenase (IDO).(66,67) IDO is an enzyme used by effector T cells to deplete tryptophan (critical for cells survival and longevity), an essential amino acid, and this protein is overexpressed in malignant brain tumors. (66,67) Tumors that utilize IDO deplete tryptophan from T cells forming kynurenines, which predispose an exhausted and regulatory T cell phenotype.(66,67) IDO blockers have been developed and are currently evaluated in children in early phase studies (phase I, clinical trials.gov: NCT02502708). (68)

Alternatively, other strategies discussed above have been employed to activate immunologic responses de novo against pediatric brain tumors, like cancer vaccines. The treatment consist to deliver tumor antigens to APCs allowing them to process and present these epitopes on the surface of their MHC class I and II molecules for presentation to T cells. (69) Glioma associated peptide vaccines with poly-I/C have been investigated in HLA-A\*002 positive patients with DIPG and HGGs. (70) These peptides (commonly expressed in childhood gliomas) included EphA2, interleukin-13 receptor alpha, and survivin. (70) Thirteen of twenty-one children treated with these peptide vaccines had an immune response to the antigens. (70)These results are promising but HLA-A\*002 restricted constraining eligibility to patients that express this haplotype. Alternatively, DNA or RNA based vaccines bypass HLA haplotype restriction, allowing an individual's cell machinery to transcribe/translate nucleic acids into proteins for personalized processing. (71-74)



Like vaccines, oncolytic viral therapy intends to induce endogenous immune responses. (75-79) Oncolytic viruses are attenuated or genetically modified in order to preferentially propagate in tumor cells to allow the recognition of oncologic cells by the immune system for rejection. (75-79) Oncolytic viral therapy has been employed in several cancers with promising results and is currently being evaluated in phase I studies in children with recurrent supratentorial tumors (using herpes simplex virus; [clinicaltrials.gov: NCT02457845](https://clinicaltrials.gov/ct2/show/study/NCT02457845)). (80)

Nowadays, the best developing approach is the engineered chimeric antigen receptor (CAR) modified T cells, which can be utilized to target surface antigens. (81-86) Recently, in the field of CNS tumors, CAR T cells have been shown to mediate significant anti-tumor activity against adult glioblastoma by targeting HER2 or IL13Ra2, which can be employed against pediatric high-grade gliomas (phase I, [clinicaltrials.gov: NCT02208362](https://clinicaltrials.gov/ct2/show/study/NCT02208362)). (87,88) CAR T cells have the binding antibody capacity with the cytotoxicity of a T cell, with the possibility off-target side effects. (81-86)The targeting of normal antigens by CAR T cells in the brain may lead to CNS inflammation, neurotoxicity, and risks for an increased intracranial pressure and herniation. Future development of CAR T cell therapies that activate only after binding to multiple tumor surface antigens may limit these off-target effects. (89)Instead, we can genetically modified T cells in order to express an exogenous TCR with the same CAR based immunosuppressive cancer effect. Exogenous TCR are able to recognize antigens presented by MHC class I or II, thus implicating haplotypes restriction.

Other types of adoptive cell therapies for pediatric brain tumors include the transplantation of autologous/allogeneic tumor-specific cytotoxic T lymphocytes and natural killer (NK) cells. In children with posterior fossa tumors, autologous NK cells are being expanded ex vivo before intraventricular infusion (via ommaya reservoir) (phase I, [clinicaltrials.gov: NCT02271711](https://clinicaltrials.gov/ct2/show/study/NCT02271711)). Allogeneic T and NK cells are also being administered after non-myeloablative haploidentical transplant (reduced intensity conditioning regimens) to enable graft versus tumor killing against high risk solid tumors (i.e., pediatric brain tumors) (phase II, [clinicaltrials.gov: NCT01804634](https://clinicaltrials.gov/ct2/show/study/NCT01804634) and [NCT02100891](https://clinicaltrials.gov/ct2/show/study/NCT02100891)).

Synergistically approach joined with novel strategies development is the best way to

speed up the fight against pediatric brain tumors. These early phase studies are important to better understand the optimal dose, safety, and efficacy of these investigational agents. While aggressive surgical resection, radiation, and chemotherapy have improved the cure rates for many pediatric patients with malignant brain tumors, the important side effect lead to a poor patients QoL, and these cancers remain the most common cause of solid cancer death in children. (90) New targeted therapies are vital to improve treatment outcomes, but must be developed to enable trafficking across the BBB.

**Figure 2**

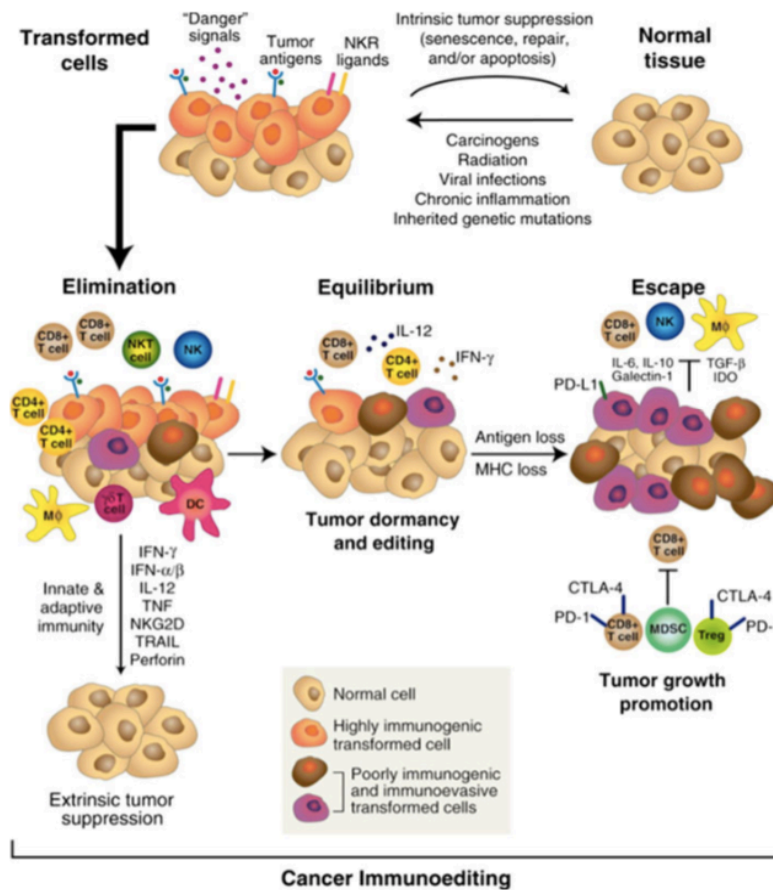


**Figure 2. Cancer immunoediting paradigm.** It defines the dynamic relationship between tumor development and anti-tumor immunity. (92)

### **1.5.A New Target for MB Immunotherapy: PRAME**

Cancer cells must be recognized from their surrounding environment to allow adoptive T cell immune mediated tumor toxicity. Nowadays, a well-established characterization of TAAs is critical for the correct development of new strategies in order to obtain a potential tumor-specific antigenic repertoire. Due to brain complexities, it is fundamental to discard immunological off-targets. In MB contest, among the potential tumor antigens, some of the best typified are the so-called cancer testis antigens (CTAs).(93,94) CTAs (the most common are MAGE and GAGE proteins) were initially described in melanoma, where they were able to trigger an autologous T-cell-mediated anti-tumor response. CTAs are proteins normally expressed in normal male germ cells but over-expressed in several types of cancer cells and not in usual somatic cells, (95) CTAs are considered efficient biomarkers to target cancer cells due to their expression pattern and to develop immunotherapy strategies. (96,97) CTAs constituted an enormous genes' family of closely associated members and are classified into two groups: the CT-X antigens that are encoded by the X chromosome and the non-X CTAs that are encoded by the autosomes. To date, 228 CTAs have been discovered: 120 CTAs (52%) map to the X chromosome, while all the others are present on the autosomes and Y chromosome. (98,99) Starting from melanoma, these antigens were also found being over-expressed in different cancer types like breast cancer, lung cancer, esophageal cancer, hepatocellular carcinoma, Acute Lymphoblastic Leukemia, and MB and their expression correlates with aggressive tumor phenotype and resistance to chemotherapy. (93) MB treated with current therapies exhibits compliances due to the severity of the treatment itself and is an ideal target for immunotherapy development. In the previous paragraph, we showed the feasibility of this strategies in the context of brain tumors, where immunotherapies are already been applied but improvement are necessary. These “biological technologies” has the potentiality to improve the current outcome in MB high risk patients. It is more effective in killing tumor cells and less toxic for the brain development than the current treatments.

Recently, Amir Al et al, discovered a new HLA-A\*002 restricted TCR able to recognize the preferentially expressed antigen in melanoma (PRAME) with high

affinity. (100) They showed the great capacity of this selected TCR to recognize and trigger an immune response against cells expressing PRAME. PRAME belongs to the cancer-testis antigens (CTA) family, and its expression has been demonstrated in several tumors (including melanoma, non-small cell lung carcinoma, breast carcinoma, renal cell carcinoma, head and neck cancer, Wilms' tumor and Hodgkin's lymphoma) and in germ-line tissues, whereas it has limited expression in healthy adult tissues. (101)

PRAME may be explored for its feasibility of adoptive T cells immunotherapy for treatment of patients with MB, studying its up-regulation in this malignancy.

PRAME was originally identified as a gene coding for HLA-A\*024-presented antigens, able to stimulate tumor-specific cytotoxic lymphocytes (CTL) derived from melanoma patients. (102) PRAME is a protein of 509 amino acids with uncertain function that is encoded by the PRAME gene located on chromosome 22 (22q11.22).(102) Few quantities of PRAME transcripts were displayed by trophoblasts and testis, normal adrenal, ovarian and endometrial cells. It is demonstrated that a clinically relevant characteristic of PRAME protein is an immunogenic nonapeptide able to induce a cytotoxic activity by T cells when presented by HLA-A24, thus, inspiring a potential role of PRAME as a target for immunotherapy.(102) Recently, a study of the PRAME physiologic role demonstrates that overexpression of this protein confers growth or survival advantages by antagonizing Retinoic Acid Receptor (RAR) signaling (103), and is causally involved in tumorigenic process. These features make PRAME a suitable target antigen for tumor immunotherapy. (104,105) Despite the possibility of *in vitro* reactivation of T cells progenitors specifically directed against PRAME peptides able to target leukemia HLA- matched cells (106-108), this approach remains difficult to translate into clinical application, for several reasons, including the scarce availability of “clinical grade” reagents, (produced with good laboratory procedures in compliance with “Good Manufacturing Practices”(GMP));the need to generate autologous antigen-presenting cells, as well as, the prolonged *in vitro* culture needed to generate clinically meaningful numbers of specific T cells.

## 2. AIMS OF WORK

We chose to focus our project on PRAME as a target for an immunotherapy approach in patients with MB.

To this end, the following aims were pursued:

- Evaluation of PRAME expression in MB subgroups and its correlation with survival rate and patients outcome.
- Cloning of a HLA-A\*002<sup>+</sup>-restricted  $\alpha\beta$ TCR specific for SLLQHLIGL PRAME-derived peptide (SLL-TCR) to target HLA-A\*002<sup>+</sup> MB tumor cell lines.
- Evaluation of *in vitro* functionality of SLL-TCR T cells against HLA-A\*002<sup>+</sup> MB tumor cell lines.
- Development of a xenograft orthotopic mice model to assess the *in vivo* anti-tumor activity of SLL-TCR T cells towards MB tumor.

## **3. Materials and Methods**

### **3.1. Cell lines**

The following cell lines: DAOY (desmoplastic cerebellar medulloblastoma, HLA-A\*02+), D283 Med (medulloblastoma, down-regulated HLA-A\*02), CEMT2 (hybrids of human T and B lymphoblastoid cell lines, HLA-A\*02+), RS4:11 (acute lymphoblastic leukemia, HLA-A\*02-), U266 (myeloma, HLA-A\*02+), HDML2 (Hodgkin lymphoma, HLA-A\*02-) and HEK 293T/17 (Embryonic Human Kidney used to produce retroviral supernatant), were obtained from the American Type Culture Collection Company (ATCC). RS4:11, U266, HDML2 and CEM-T2 were maintained in culture with RPMI 1640 medium (EuroClone, Italy). DAOY and D283 MB cells were cultured in IMDM medium (EuroClone, Italy), while HEK 293T/17 in DMEM medium (EuroClone, Italy). Mediums contain 10% heat-inactivated, fetal bovine serum (EuroClone, Italy), 2 mM L-glutamine (GIBCO, USA), 25 IU/mL of penicillin, and 25 mg/mL of streptomycin (EuroClone, Italy). Cells were maintained in humidified atmosphere containing 5% CO<sub>2</sub> at 37°C. Identity of all cell lines was confirmed by an external lab (BMR Genomics srl) through PCR-single-locus-technology (Promega, PowerPlex 21 PCR); mycoplasma test was performed every three months.

### **3.2. Healthy Donor's PBMCs, MB patients and controls**

Peripheral blood mononuclear cells (PBMC) were isolated from either peripheral blood (PB) or buffy coat obtained from 8 healthy donors after obtaining written informed consent, in accordance with rules set by the Institutional Review Board (IRB) of Bambino Gesù Children's Hospital of Rome (OPBG) (Approval of Ethical Committee N°969/2015 prot. N° 669LB), using Lymphocyte Separation Medium (Eurobio; France). MB specimens were obtained from a cohort of 60 patients with histologically-confirmed diagnosis who had undergone surgical resection at the OPBG between August 2011 and April 2015. All specimens were formalin-fixed, sectioned, stained with hematoxylin and eosin (H&E) and examined through

microscopy. In order to minimize inter-observer variability, histology was reviewed by an experienced neuropathologist, F.G., according to the international staging system for pediatric brain tumors. (109,110) The investigation was approved by the Institutional Review Board (Prot. N. 21LB; Study N 730/2013 OPBG). Informed consent was obtained from patient's parents or legal guardians (as required per institutional review board policy). For all samples, around 0.5 cm<sup>3</sup> of tumor's tissue was also snap-frozen in liquid nitrogen and stored at -80°C until ready for RNA extraction. Clinical (age, gender and outcome), molecular and histopathological details of all 60 patients and of the 51 of them followed in our Institution are reported in Table 1. RNA of normal human cerebellum (10 adult samples from 25- to 70-year-old subjects and 8 samples from 22 to 36-week-old foetuses) was purchased from Biocat (Heidelberg, Germany), Ambion (USA) and BD Biosciences (USA). MB primary cell lines were obtained from fresh patient's tissue samples. In detail, tissues were collected in HBSS media (Thermo Fisher Scientific, USA) supplemented with 0.5% glucose and 2% Penicillin/Streptomycin, grossly triturated with serological pipette and treated with DNase-I (Sigma-Aldrich, United Kingdom) to a final concentration of 0.04% for 20 min. Finally, cells aggregates were mechanically dissociated using pipettes of decreasing bore size to obtain a single-cell suspension that was grown in DMEM/F12 medium + 10% FCS and 2% Penicillin/Streptomycin at 5% CO<sub>2</sub>. After 1 week, the supernatant was removed from cultures and replaced with fresh medium. Two weeks after the start of the culture, cells were harvested and characterized for the expression of PRAME and neural markers (B3TUBB, S100A, GFAP) and re-plated to perform the experiments. In selected experiments, cell lines or primary MB patient-derived cells were pre-treated with 1,000 IU/mL of IFN $\gamma$  (R&D System, USA) for 48 hours before their use as target cells.

### **3.3. Retroviral constructs**

The complete PRAME specific  $\alpha\beta$ TCR recognizing SLL-peptide in the context of HLA-A\*02 (100) was cloned in a retroviral vector containing in frame the iC9 suicide gene sequence (iC9-SLL TCR). An additional retroviral vector encoding eGFP-Firefly-Luciferase (eGFP-FFLuc) (111) was used in selected experiments to label



tumor cells (DAOY-FF-Luc.GFP and RS4:11- FF-Luc.GFP) for *in vitro* and *in vivo* studies, as previously described.(112)

### **3.4. Generation and expansion of polyclonal iC9-SLL TCR T cells**

T lymphocytes were activated with immobilized OKT3 (1 µg/ml, e-Bioscience Inc., USA) and anti-CD28 (1 µg/ml, BD Biosciences, USA) antibodies in the presence of recombinant human interleukin-2 (IL-2, 100 U/ml; R&D, USA). Activated T cells were transduced on day 3 in 24-well plates pre-coated with recombinant human RetroNectin (Takara-Bio, USA), using a SFG retroviral supernatant specific for iC9-SLL TCR. On day 5 from transduction, T cells were expanded in “complete medium” containing 45% RPMI1640 and 45% Click’s medium (Sigma-Aldrich, United Kingdom) supplemented with 10% FBS and 2 mM Glutamax, and fed twice a week with IL-2 (50U/ml). In selected experiments, iC9-SLL TCR T cells were generated from CD8<sup>+</sup> or CD4<sup>+</sup> T cells prepared by positive immunomagnetic sorting (MiltenyiBiotec, Germany), following the manufacturer's instructions. iC9-SLL TCR T cells were also sorted by anti- Allophycocyanin (APC) magnetic microbeads (MiltenyiBiotec, Germany), to select T cells previously stained with SLL-dextramers conjugated with APC (JPT, Germany).

### **3.5. Activation of the suicide gene**

The chemical inducer of dimerization (CID) (AP1903; ARIAD Pharmaceuticals, USA) was kindly provided by Bellicum Pharmaceuticals (Houston, Texas, USA) and added at the indicated concentrations to either control T cells or iC9-SLL TCR T cells. The elimination of transgenic cells co-expressing the iC9 suicide gene was evaluated 24 to 48 hours later by FACS analysis, enumerating the percentage of AnnexinV-/- AAD- Vβ1<sup>+</sup> CD3<sup>+</sup> T cells in the culture.

### **3.6. Immunophenotyping**

Expression of cell surface molecules was evaluated by flow-cytometry using standard methodology. The following monoclonal antibodies (mAbs) were used: SLL dextramer conjugated with APC (JPT, Germany); CD3 peridinin chlorophyll protein (PerCP)-conjugated monoclonal antibody; CD8 fluorescein isothiocyanate (FITC)-conjugated monoclonal antibody; T- cell receptor-V $\beta$ 1 phycoerythrin (PE)-conjugated monoclonal antibody (all Ab were purchased from Becton Dickinson, USA). Control samples, labeled with an appropriate isotype-matched antibody, were included in each experiment. Samples were analyzed with a BD LSRFortessa X-20. Flow cytometry profiles were analyzed using the FACSDiva software (BD Biosciences). For each sample, we analyzed a minimum of 100,000 events.

### **3.7. ELISpot assay**

We used an IFN $\gamma$  ELISpot assay, as previously described. (66) Briefly, iC9-SLL TCR T cells were plated in triplicate, serially diluted from  $1 \times 10^5$  to  $1 \times 10^4$  cells/well, and then CEM-T2 (at the ratio 1:1) loaded with either the specific SLL peptides or ALY-PRAME-derived irrelevant peptide were added at the indicated concentration (all peptides from JPT were dissolved in DMSO as indicated by the manufacturer). As a positive control, T cells were stimulated with 25 ng/mL of phorbolmyristate acetate (PMA) and 1  $\mu$ g/mL of ionomycin (Sigma-Aldrich, United Kingdom). The IFN $\gamma$ + spot-forming cells (SFCs) were enumerated (ZellNet, USA).

### **3.8. Co-Culture assays**

For co-culture experiments, un-transduced control (CNT) and iC9-SLL TCR T cells were plated at  $0.5 \times 10^6$  cells/well in 24-well plates at the indicated Effector:Target (E:T) ratios (1:1 and 5:1). Following 7 days of incubation at 37°C, adherent tumor cells and T cells were collected, and both residual tumor cells and T cells assessed by FACS analysis based on CD3 expression (Effector T cells) and GFP [(DAOY-FF-Luc.GFP cell line (PRAME+HLA-A\*02+) and RS4:11- FF-Luc.GFP cell line (PRAME+HLA-A\*02neg.ve)].

### **3.9. IFN $\gamma$ , IL2, TNF $\alpha$ ELISA**

Supernatant from Effector/Target co-culture was collected at 24 hours to measure IFN $\gamma$ , IL2 and TNF $\alpha$  released by iC9-SLL TCR T or NT T cells. The supernatant was analyzed by ELISA assay (R&D System, USA), following the manufacturer's instructions.

### **3.10. Chromium-release assay**

The cytotoxic specificity of T cells was evaluated using a standard 4- hour <sup>51</sup>Cr-release assay. Target cells were incubated in medium alone or in 1% Triton X-100 (Sigma-Aldrich, UK) to determine spontaneous and maximum <sup>51</sup>Cr release, respectively. iC9-SLL TCR T cells or NT T cells were plated in triplicate on PRAME+ HLA-A\*02+ target cells [DAOY, CEM- T2 or CEM-T2 SLL (loaded with SLL-PRAME peptide) cell line] or on PRAME+ HLA-A\*02- target cells (RS4:11 and D283). In selected experiments, we used sorted CD8+ T cells transduced with iC9-SLL TCR as effector cells. After 6 hours of co-culture of effector and target cells, as described previously (106), the supernatant was collected and radioactivity measured with a gamma counter. The mean percentage of specific lysis of triplicate wells was calculated as follows:  $[(\text{Experimental release} - \text{spontaneous release}) / (\text{maximal release} - \text{spontaneous release})] \times 100$ .

### **3.11. RNA isolation and quantitative Real-Time PCR**

Total RNA was purified and reverse transcribed (Thermo Scientific, USA) as previously described.(19,20) Quantitative RT-PCR (qRT-PCR) was performed employing Viia7 Sequence Detection System (Thermo Scientific, USA), using best coverage TaqMan gene expression assays, specific for each mRNA analysed (PRAME,  $\beta$ III-tubulin S100A, GFAP, GAPDH,  $\beta$ -ACTIN, and  $\beta$ 2-MICROGLOBULIN). Expression signature for MB sub-grouping was performed by qRT-PCR using TaqMan probes. TaqMan Low Density Array was custom-designed with TaqMan assays for genes of interest. Each amplification was performed in triplicate, and the average of the three threshold cycles was used to calculate the amount of transcripts (Thermo Scientific, USA). Transcript quantification was expressed in arbitrary units

(AU) as the ratio of the sample quantity to the mean values of control samples (PBMCs of 8 healthy donors). Relative gene expression was calculated using the  $2^{-\Delta\Delta Ct}$  method, where  $\Delta Ct$  indicates the differences in the mean cycle threshold (Ct) (113) between selected genes and three endogenous gene controls (GAPDH,  $\beta$ -ACTIN, and  $\beta 2$ -MICROGLOBULIN; data were shown only with respect to  $\beta$ -ACTIN normalization).

### **3.12. Molecular detection of retroviral transduced T cells**

Total DNA was purified according to manufacturer indications (Qiagen, USA). Retroviral vector was amplified by using TaqMan probe/primers directed towards an invariant region of the plasmid located between LTR and the transgene iC9-SLL TCR. Vector copy numbers for cells were normalized with respect to the copy numbers of the housekeeping gene  $\beta$ -Actin.

### **3.13. Xenograft mouse model for *in vivo* studies**

All immunocompromised NSG (NOD scid gamma) mice (strain NOD.Cg-Prkdcscid Il2rgtm1Wjl/SzJ) were purchased from Charles River and maintained in the animal facility at Sapienza University (where orthotopic models using stereotaxic MB implantation in mouse brains were performed) or in Plaisant Castel Romano (where Intraperitoneal (i.p.) model for the bioluminescence monitoring of the tumour using IVIS Image System was performed) in Rome. All procedures were performed in accordance with the Guidelines for Animal Care and Use of the National Institutes of Health (Ethical committee for animal experimentation Prot. N 03/2013 for University of Rome Sapienza, and Prot. N 088/2016-PR for Plaisant Castel Romano, respectively). For the orthotopic *in vivo* model, adult female NSG mice were anesthetized by intraperitoneal injection of ketamine (10 mg/kg) and xylazine (100 mg/kg). The posterior cranial region was shaved and placed in a stereotaxic head frame. DAOY cells were prepared from fresh culture to ensure optimal viability. MB cells ( $2 \times 10^5$  per 5  $\mu$ l) were stereotaxically implanted into the cerebellum at an infusion rate of 1  $\mu$ l/min by using the following coordinates, according to the atlas of Franklin and Paxinos: 6.6 mm posterior to the bregma; 1 mm lateral to the midline; and 2 mm ventral from the surface of the skull. After injection, the cannula was kept in place for about 5 min for equilibration of pressures within the cranial vault. The skin

was closed over the cranioplastic assembly using metallic clips. Ten days following tumor implantation, the animals were randomly divided into three groups: Group 1 = intracranial injection of CTRL -T lymphocytes; Group 2: intracranial injection of PRAME-T lymphocytes; Group 3: no lymphocyte injection. In selected experiments, T cells were inoculated intravenous (i.v.) into the tail vein. On the same day of T-cell infusion, IL2 i.p. treatment was started (1.000 U/animal in PBS; administered twice a week). After 4 weeks, animals were sacrificed and brains were fixed in 4% formaldehyde in 0.1 M phosphate buffer (pH 7.2) and paraffin embedded. For brain tumor volume calculation, serial thick coronal sections (2  $\mu$ m) starting from the mesencephalon to the end (HALF) of cerebellum were performed. In order to *in vivo* estimate tumor control within a setting of bulky tumor, we also carried out an i.p. model of MB. In particular, in NSG male mice of 5 weeks age, we engrafted i.p.  $2 \times 10^6$  PRAME+ tumor cells (DAOY-FF-Luc.GFP) re-suspended in Matrigel (Becton Dickinson, USA). Ten days later, when the light emission of the tumor was consistently measurable, mice received i.p. injection of  $10^7$  iC9-SLL TCR T cells or control, un-transduced T cells. Tumor growth was evaluated using IVIS imaging system (PerkinElmer, USA). Briefly, a constant region of interest was drawn over the tumor regions and the intensity of the signal measured as total photon/sec/cm<sup>2</sup>/sr (p/s/cm<sup>2</sup>/sr), as previously described.(24) For *In vivo* CID study, we genetically modified T cells (CNT and iC9-SLL TCR T cells) to express the Fire Fly luciferase and these cells monitored through IVIS technologies (DAOY cell line was wt and stereotaxically implanted). After 4 days, the drug AP1903 (100mg/mouse) was infused and mice analyzed for the iC9-SLL TCR T cells presence.

### **3.14. Histological and immunohistochemistry data**

The histopathologic H&E analysis for the orthotopical models was performed on 40 sections (2  $\mu$ m each), sampled every 40  $\mu$ m on the horizontal plan of the cerebellum, in which the cerebellum was identified and outlined at 2.5x magnification. Tumor area of every slice was evaluated with a microscope (Axio Imager M1 microscope; Leica Microsystems GmbH, Germany) equipped with motorized stage and Image Pro Plus 6.2 software. The following formula was used to calculate the mouse brain tumor volume: tumor volume = sum of measured area for each slice x slice thickness x

sampling frequency. For immunohistochemistry (IHC) analysis, the sections were deparaffinized with xylene, sequentially rehydrated in ethanol, and incubated in 0.3% hydrogen peroxide for 10 minutes to quench endogenous peroxidase activity. Immunostaining was performed using the Vectastain Elite ABC kit (Vector Laboratories, Burlingame, CA). Nonspecific binding was blocked by incubation with normal rat serum for 30 minutes. The sections were then incubated with anti-CD3 antibody (1:100, DAKO) or anti-PRAME (1:100, ABCAM) at 4°C for 60 minutes. Sections were incubated with a biotinylated secondary antibody (anti-mouse or anti-rabbit IgG) for 30 minutes, washed, and incubated for another 30 minutes with ABC (avidin and biotinylated enzyme complex) reagent. Colour was developed by adding peroxidase substrate diaminobenzidine. Sections were counterstained with Mayer's hematoxylin (Sigma-Aldrich) and, finally, mounting solution and coverslips were added.

### **3.15. Mouse behavioural studies**

Mice were stereotaxically implanted with DAOY ( $0.2 \times 10^6$ /mouse). Ten days after, CNT or iC9-SLL TCR T cells ( $1 \times 10^7$  cells/mouse) were inoculated i.v. into the tail vein. To evaluate the neurological effect of potential side effects due to T cell expansion, beginning on day before T cell infusion, throughout the period of tumor eradication (day 14), all the animals ( $n=8$ ; 4 in each cohort of treatment) were assessed using a modified Smith-Kline Beecham, Harwell, Imperial College, Royal London Hospital, phenotype assessment (SHIRPA) protocol (114). This comprehensive behavioural assessment involves a battery of 33 semi-quantitative tests for general health and sensory function, baseline behaviours and neurological reflexes. The procedures were carried out in an open testing environment away from the home cage, and took 15–20 min per animal daily.

### **3.16. Statistical analysis**

All data are presented as means  $\pm$  SD. Student t test was used to determine the statistical differences between samples, and p value  $<0.05$  was considered to be statistically significant. Maximum likelihood method (115) using R2: Genomics Analysis and Visualization Platform (<http://r2.amc.nl>) was applied to calculate the expression level of  $19.2 \times 10^3$  AU as cut-off to stratify patients based on PRAME

expression. The Kaplan-Meier method was used to estimate overall survival (OS) probabilities; differences between groups were compared with the log-rank test. Hazard ratio for death was calculated with 95% confidence interval (CI). No evaluable samples were excluded from the analyses. Animals were excluded only in the event of death after tumor implant, but before T-cell infusion. Neither randomization nor blinding was done during the *in vivo* study. However, mice were matched based on the tumor signal for control and treatment groups before infusion of control or gene-modified T cells in the i.p. bulky MB tumor model. In this last model, to evaluate tumor growth over time, bioluminescence signal intensity was collected in a blind fashion. Bioluminescence signal intensity was log transformed and then compared using a two-sample t-test. The analysis of the neuropathologist (F.G.), aimed at quantifying tumor volume, was performed in a blind fashion. We estimated the sample size considering the variation and average of the samples. We tried to reach a conclusion using a sample size as small as possible. We estimated the sample size to detect a difference in averages of 2 standard deviation at the 0.05 level of significance with an 80% power. Graph generation and statistical analyses were performed using Prism version 6.0d software (GraphPad, USA).

## 4. Results

### 4.1. PRAME expression in MB at diagnosis and relapse

We evaluated CTAs gene expression data-sets through bioinformatics analysis. The data evidenced that the majority of known CTAs are either downregulated or not modulated (figure 3A and B) in MB samples respect to normal cerebellum. Only CTAs PRAME (Figure 3C) and CT22 (a CT-antigen, also known as Sperm Autoantigenic Protein 17 - SPA17, with a wide expression in somatic tissues) have a different expression pattern. (116) Starting from these observations, we decided to focalize our attention on PRAME, analyzing its mRNA expression levels in 10 normal adult (NAHC) and 8 foetal cerebella (NFHC), underlining a less expression than mononuclear cells derived from 8 healthy donors (PBMC, Figure 4A). We then studied PRAME mRNA levels in tumor samples collected at diagnosis from 60 MB patients diagnosed/treated at OPBG. The clinical-pathological data of the considered MB patients are summarized in Table 1. The 82% (49 out of 60) of all tumor samples showed a significative higher PRAME expression (average  $92,2 \times 10^3 \pm 248 \times 10^3$ ; range,  $0,9 \times 10^3 - 1500 \times 10^3$  AU) respect to NAHC tissues (average,  $0,8 \times 10^3$  AU;  $p < 0,0001$ ), with no relevant differences among the four molecular subgroups (Figure 4A). Noteworthy, Kaplan–Meier analysis evidenced that high PRAME mRNA expression correlates significantly with a worse Overall Survival (OS) probability in the 51 patients for which follow-up data were available in our Institution. This correlation remains statistically significant considering the PRAME mRNA expression cut-of as the maximum likelihood estimation threshold (117) of  $19,2 \times 10^3$  AU ( $p = 0,0004$ ; Figure 4B), the median value of  $7,705 \times 10^3$  AU ( $p = 0,0003$ ; Figure 4E), the first quartile value of  $0,381 \times 10^3$  AU ( $p = 0,002$ ; Figure 4F) and third quartile value of  $36,221 \times 10^3$  AU ( $p = 0,0006$ ; Figure 4G) quartile. Indeed, the median overall survival was 29.1 months (95% CI, 6 to 62) in high-PRAME-expressing patients group versus 59.4 months (95% CI, 6 to 158) in low-PRAME-expressing patients group ( $p = 0,0004$ ; Figure 2B. Hazard ratio for death, 4.258; 95% CI, 2.288 to 15.39;  $p = 0,0031$ ). Considering patients according to the four molecular subgroup, we verified a significant correlation between high PRAME expression and worse OS in SHH-MB (n=9; Figure 4C,  $p = 0,0038$ ) and G3-MB (n=19; Figure 4D,  $p = 0,0075$ ) subgroups; this



correlation was not statistically significant in WNT-MB (n=9) and G4-MB (n=14) due probably to the low number of patients studied. PRAME expression also correlated in our patient's cohort with male gender ( $p=0.0279$ ). We also analyzed PRAME expression in two MB patients (one case of SHH-MB and one of Group 3-MB) for which tumor biopsies were available both at diagnosis and at time of relapse, demonstrating high level of the antigen in recurrent MBs (Figure 5A). After all, IHC analysis shows relevant PRAME protein expression in MB tumour samples, ranging from 20% to more than 90% of positivity in tumour cells, whereas the expression of PRAME protein were negligible in normal brain (Figure 5B).

**Table1**

Summary of the clinical, pathologic, and molecular features of patients with medulloblastoma investigated for PRAME expression

Variable	No. of Dx n = 60	PRAME Expression		P X <sup>2</sup> test	PRAME Expression			P X <sup>2</sup> test
		HIGH <sup>a</sup> n = 23	LOW <sup>b</sup> n = 37		No. of MB pts with known FU n = 51	HIGH <sup>a</sup> n = 19	LOW <sup>b</sup> n = 32	
Age				0.4199				0.2108
Infant (≤ 3 years)	12	4	8		9	5	4	
Children (> 3 years ≤ 17 years)	47	18	29		42	14	28	
Adults (>17 years)	1	1	0		0	0	0	
Gender				0.0279				0.0459
Male	39	11	28		33	9	24	
Female	21	12	9		18	10	8	
Molecular subgroup				0.6342				0.5307
WNT	10	4	6		9	4	5	
SHH	14	6	8		9	4	5	
Group 3	20	9	11		19	8	11	
Group 4	16	4	12		14	3	11	
Histology				0.1422				0.188
Desmoplastic	11	4	7		9	2	7	
Classic	36	11	25		30	10	20	
Anaplastic/large cell	13	8	5		12	7	5	
Tumor material				0.0681				0.0612
Primary	58	21	37		49	17	32	
Recurrence	2	2	0		2	2	0	
Status				0.001				0.001
Dead	20	13	7		20	13	7	
Alive	31	6	25		31	6	25	
Alive with <5 year FU	9	4	5					

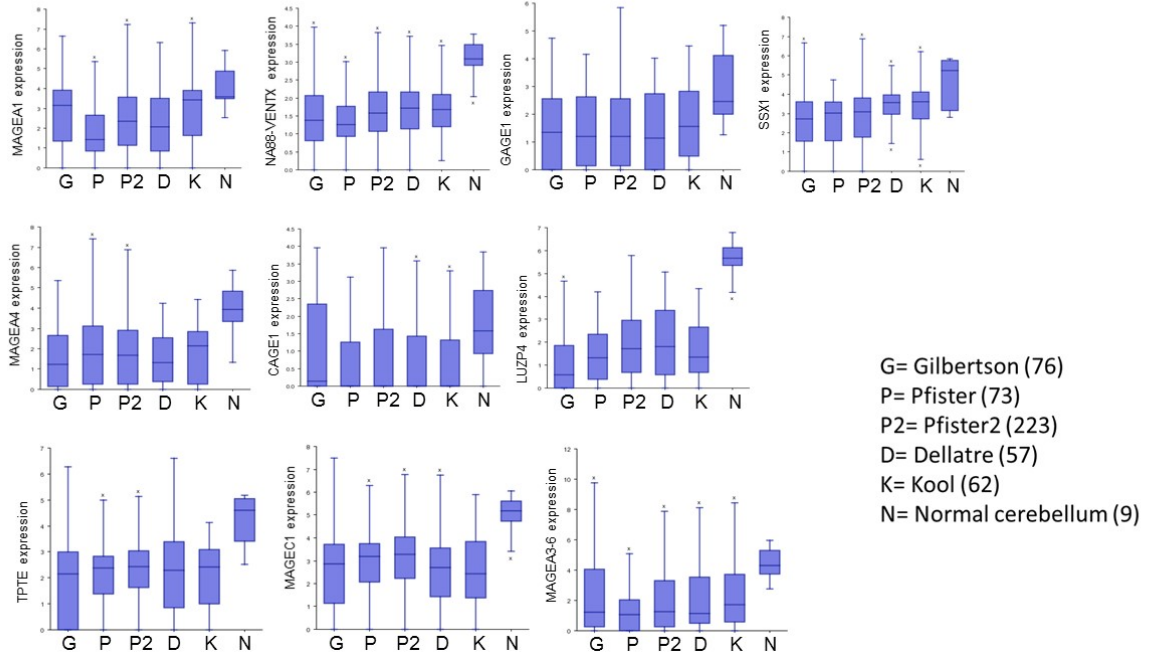
Abbreviation: FU, follow-up.

<sup>a</sup>High PRAME expression > 19.2 × 10<sup>3</sup> AU.

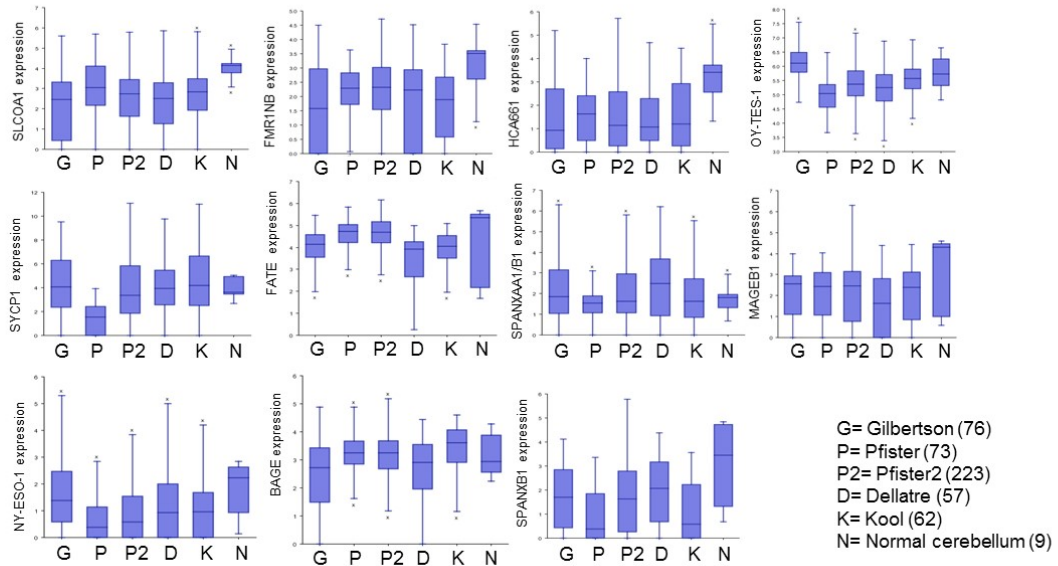
<sup>b</sup>Low PRAME expression < 19.2 × 10<sup>3</sup> AU.

**Figure 3**

**A**

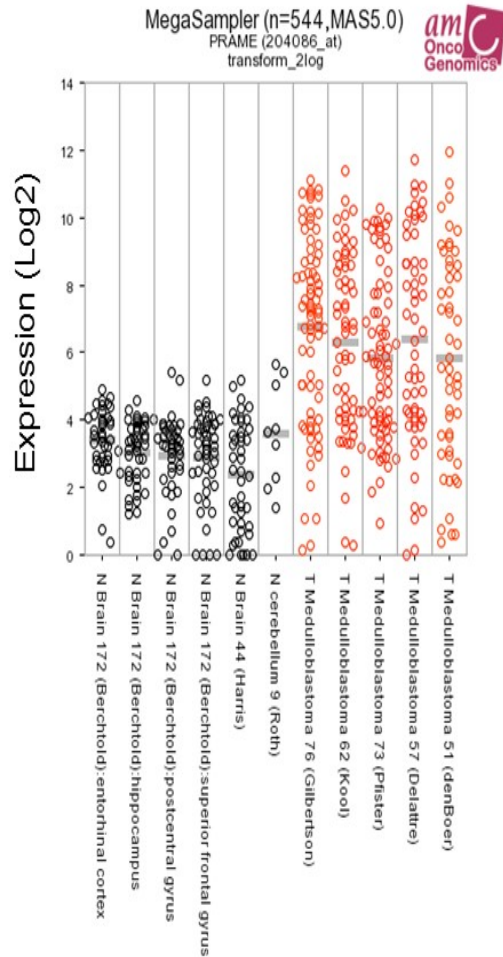


**B**



C

1



2

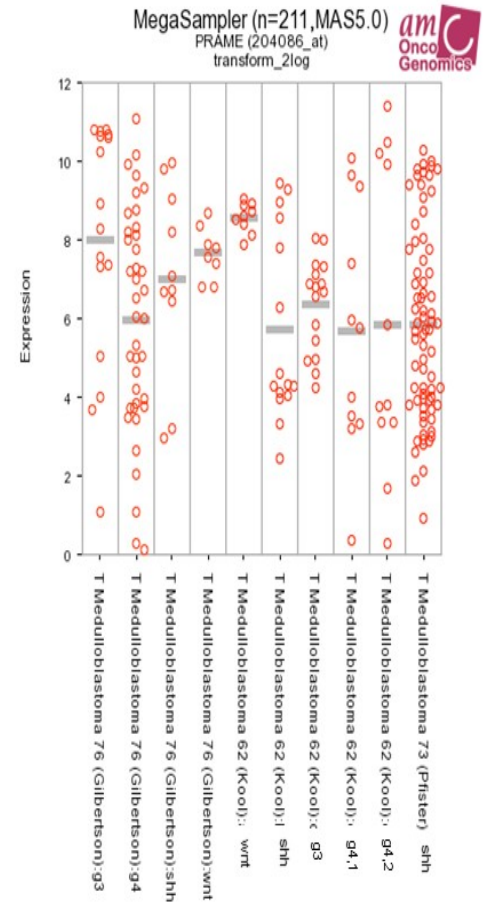


**Figure 3.A, CTA down modulated in MB respect normal cerebellum.** CTA mRNA gene expression profiles across Gilbertson (GEO ID: GSE37418), Kool (GEO ID: GSE10327), Pfister (P=GEO ID: GSE49243; P2=ps\_avgpres\_mb500affym223\_u133p2), Fattet/Delattre (GEO ID: GSE74195) datasets exploring CTA expression in either normal brain (N) or patients with MB. Numbers in the legend indicate the number of samples evaluated in each dataset. We have included in the analysis the following CTAs: MAGEA1 (melanoma antigen family A1), NA88 – VENTX (VENT homeobox), GAGE1 (G Antigen 1), SSX1 (synovial sarcoma, X breakpoint 1), MAGEA4 (melanoma antigen family A4), CAGE1 (cancer antigen 1), LUZP4 (leucine zipper protein 4), TPTE (Transmembrane phosphatase with tensin homology), MAGEC1 (melanoma antigen family C1) and MAGEA3-6 (melanoma antigen family A3/6). **B, CTA not modulated in MB respect normal cerebellum.** CTA mRNA gene expression profiles across Gilbertson (GEO ID: GSE37418), Kool (GEO ID: GSE10327), Pfister (P=GEO ID: GSE49243; P2=ps\_avgpres\_mb500affym223\_u133p2), Fattet/Delattre (GEO ID: GSE74195) datasets exploring CTA expression in either normal brain (N) or patients with MB. Numbers in the legend indicate the number of samples evaluated in each dataset. We have included in the analysis the following CTAs: SLCO6A1 (Solute carrier organic anion transporter family, member 6A1), FMR1NB (fragile X mental

retardation 1 neighbor), HCA661 (transcription factor Dp family, member 3), OY-TES-1 (ACRBP, acrosin binding protein), SYCP1 (synaptonemal complex protein 1), NY-ESO-1, FATE (fetal and adult testis expressed 1), SPANXA1/B1 (Sperm protein associated with the nucleus, X-linked, family member A1), MAGEB1 (melanoma antigen family B1GAGE1), BAGE (B melanoma antigen), SPANXB1 (family member B1). **C, PRAME mRNA expression data from public datasets of expression profiles in MB patients.** (1) PRAME mRNA gene expression profiles across Gilbertson (GEO ID: GSE37418), Kool (GEO ID: GSE10327), Kool/Pfister (GEO ID: GSE49243), Fattet/Delattre and de Bont (GEO ID: GSE74195) datasets exploring PRAME expression in either normal brain (black plot circles) or patients with MB (red plot circles). Numbers indicate the number of samples evaluated in each dataset. (2) PRAME mRNA gene expression profiles across Gilbertson, Kool and Pfister datasets, exploring PRAME expression in patients with different MB-subtypes. Numbers indicate the number of samples evaluated in each MB subtype.

**Figure 4**

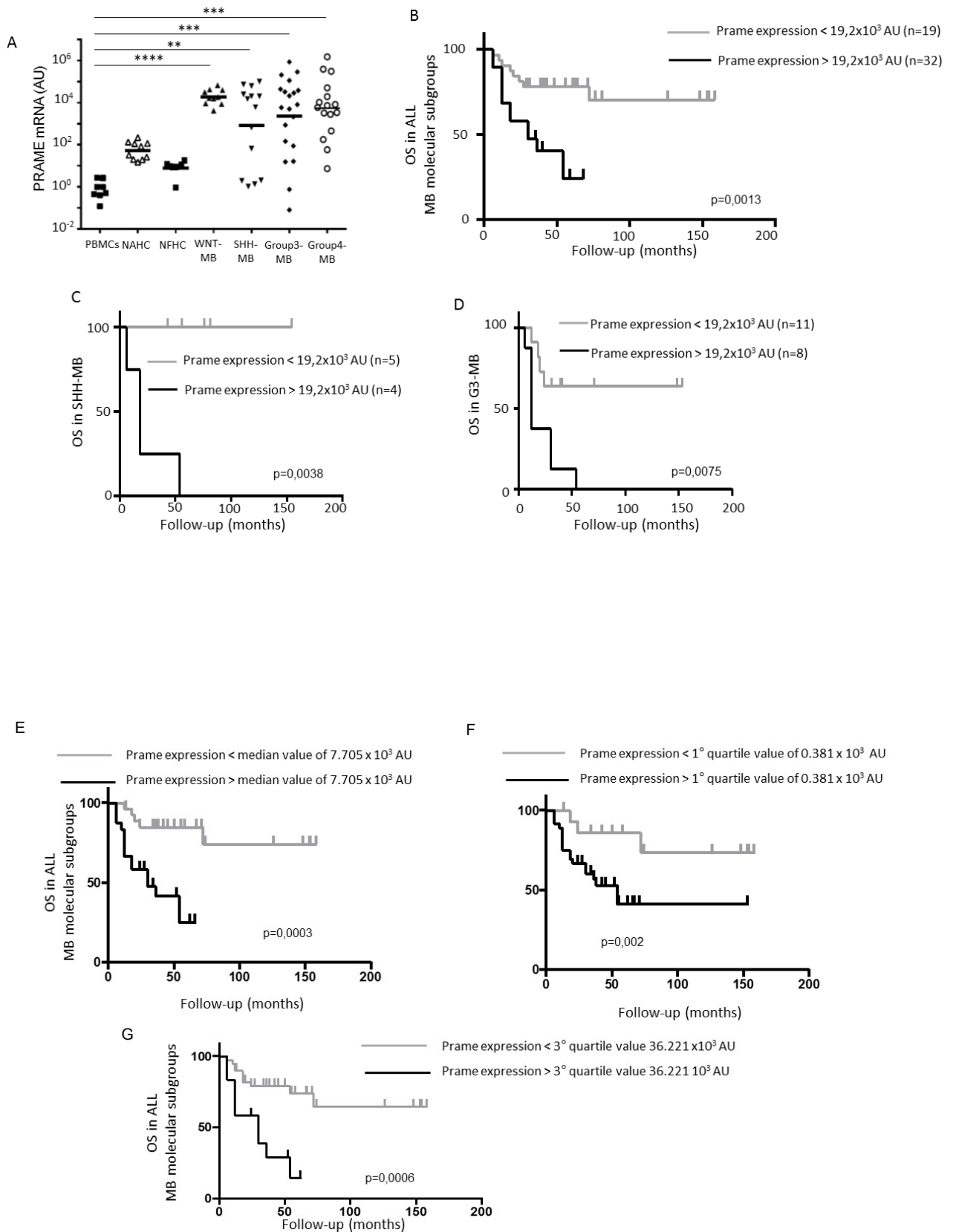
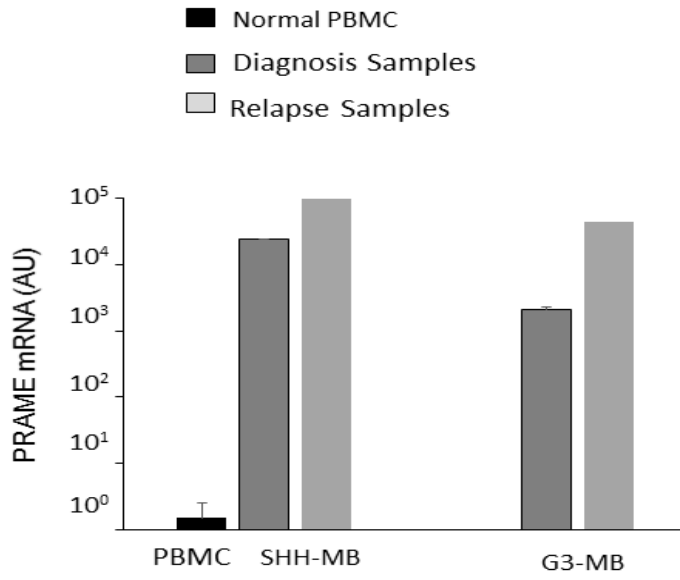


**Figure 4. PRAME mRNA expression and its correlation with clinical feature of MB.****A**, Relative expression of PRAME mRNA in PBMCs isolated from 8 healthy donors, 10 normal adult human cerebella (NAHC), 8 normal fetal human cerebella (NFHC), biopsies from 10 patients with WNT-MB pathway subtype, 14 patients with SHH-MB pathway subtype, 20 patients with Group 3-MB, and 16 patients with Group 4-MB. Transcripts quantification was expressed in AU versus the average expression of PRAME mRNA observed in PBMCs isolated from 8 healthy donors. \* $\leq P 0.05$ ; \*\* $\leq P 0.001$ ; \*\*\* $\leq P 0.0001$ ; \*\*\*\* $\leq P 0.00001$ . **B**, Kaplan–Meier analysis for OS in all 51 patients with MB with a known follow-up ( $n=51$ ), stratified by PRAME mRNA expression  $>19.2 \times 10^3$  AU or  $19.2 \times 10^3$  AU, respectively. Differences between groups were compared with the log-rank test. **C and D**, Kaplan–Meier analysis for OS in patients with SHH-MB (**C**) and G3-MB (**D**) with more than 5 years of follow-up ( $n=51$ ), stratified by PRAME mRNA expression  $>19.2 \times 10^3$  AU or  $19.2 \times 10^3$  AU, respectively. **E, F, G, Differential cut-off for PRAME mRNA expression and their correlation with clinical feature of MB.** Kaplan-Meier analysis for overall survival (OS) in all 51 MB patients with a known FU ( $n=51$ ), stratified by PRAME mRNA expression considering the cut-off of median value of  $7.705 \times 10^3$  AU (**E**), 1° quartile value of  $0.381 \times 10^3$  AU (**F**) or 3° quartile value  $36.221 \times 10^3$  AU (**G**), respectively. Differences between groups were compared with the log-rank test.

**Figure 5**

A



B

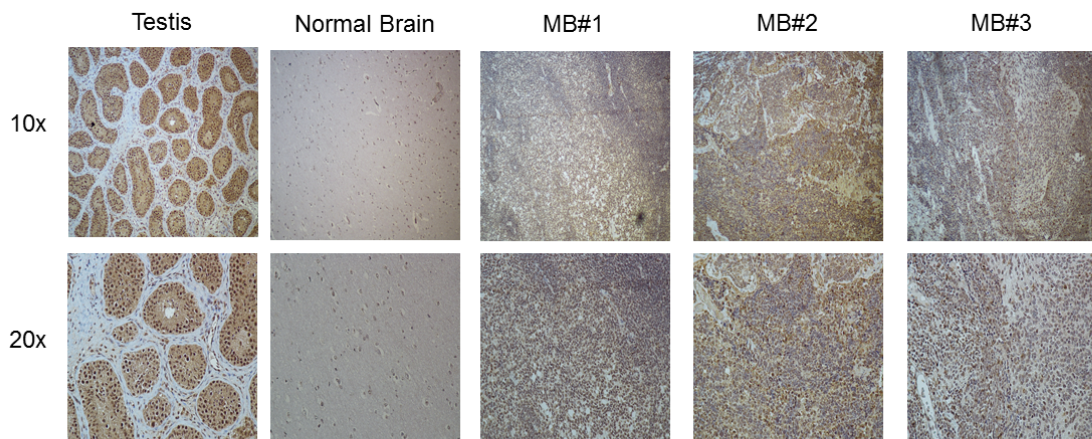




**Figure 5. A, MB tissues from two patients in relapse show high level of PRAME expression.** Relative expression of PRAME mRNA from matched primary-metastases MB tissues of patient with Group3-MB or with SHH-MB at diagnosis (dark gray bar) or at the time of relapse (light gray bars). PRAME mRNA expression in PBMC from 8 healthy donors has been added for comparison (black bars). **B, Immunohistochemistry results of histological sections to evaluate PRAME expression.** IHC images of PRAME staining of testis (positive control), normal cerebellum and three MB patients. Original magnification 10X and 20X .

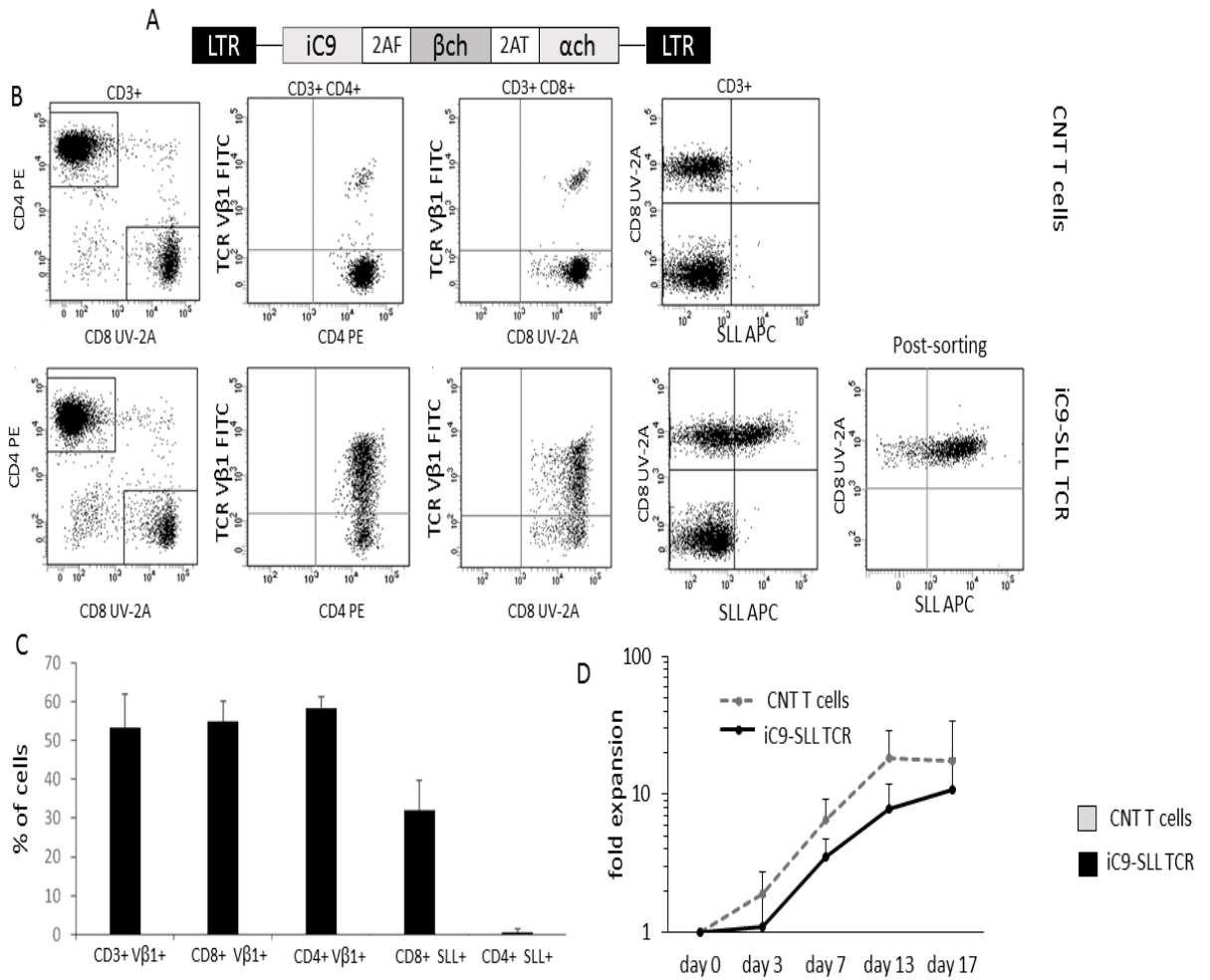
## **4.2. Retroviral vector carrying iC9 and PRAME-SLL specific $\alpha\beta$ TCR allows stable and functional expression of the transgenes.**

TCR ( $\alpha$  and  $\beta$  chains) sequences specific for PRAME-SLL in frame with iC9 sequences (100), were cloned, codon-optimized, and encoded into a retroviral vector (iC9-SLL TCR, Figure 6A). Then, primary T cells or CD8<sup>+</sup> sorted T cells (derived from PBMCs of healthy donors) were transduced with the generated retrovirus and expanded in the presence of cytokine IL2. About Six days after transduction, 53% $\pm$ 8,6% of CD3<sup>+</sup> T cells stained for TCRV $\beta$ 1 (to which PRAME-SLL TCR  $\beta$  chain belongs) and 32% $\pm$ 7,8% of CD8<sup>+</sup> T cells were detected positive for SLL dextramer (Figure 6B shows an explicative example, whereas the median level of transduction reached in 8 independent experiments is shown in Figure 6C). In particular, CD4<sup>+</sup> T cells were also significantly transduced with iC9-SLL TCR, as shown by the expression of TCRV $\beta$ 1; however, using SLL-dextramer staining, CD4<sup>+</sup> cells resulted negative for the SLL-TCR pairing, since SLL-dextramer staining is specific only for CD8<sup>+</sup> cells (Figure 6B). Moreover, no significant differences in the transduction level (considering TCRV $\beta$ 1 or dextramer staining analysis) were detectable between total T cells and CD8<sup>+</sup> selected T cells.

Starting from this observation, we decided to select through a SLL-dextramer microbeads, from the genetically modified T cells, the subset that express the correct SLL-TCR  $\alpha$  and  $\beta$  chains pairing. Our *in vitro* data demonstrated that the selected SLL-TCR<sup>+</sup> T cells stably expressed the transgene (Figure 6B) and were able to expand, generating a great number of iC9-SLL TCR T cells. Analyzing these genetically modified T cells, they showed a polyclonal phenotype after transduction, since no preferential TCR $\beta$  family usage has been observed in SLL-dextramer<sup>+</sup> T cells, beside SLL-specific V $\beta$ 1 repertoire (Figure 6E). Furthermore, no proliferative differences were found between transduced T cells or non-transduced T cells (CNT T cells) when co-cultured with the pleiotropic cytokine IL2 (10,7 $\pm$ 7,6 and 17.5 $\pm$ 16,5 fold expansion at day 15, respectively, Figure 6D). The exogenous expressed SLL TCR was functional, since iC9-SLL TCR T cells produce IFN- $\gamma$  in response to the CEM-T2 cell line loaded with the SLL peptide (until 10<sup>-5</sup> M concentration), but not with the irrelevant PRAME-peptide ALY (Figure 7A). In potency experiments, through Cr<sup>51</sup>

release assay, we demonstrated that SLL peptide-pulsed CEM-T2 cells were lysed by iC9-SLL TCR T cells at higher extent than un-loaded CEM-T2 (i.e. a HLA-A\*02+ cell line characterized by low PRAME expression, as shown in Figure 5E;  $69,8\% \pm 6.5\%$  vs  $8.0\% \pm 1.8\%$  specific lysis, respectively at the Effector:Target (E:T) ratio of 20:1,  $p \leq 0.005$  Figure 7B). Noteworthy, iC9-SLL TCR T cells, when co-cultured with the tumor cell line U266 (HLA-A02+ PRAME+) in a ratio 1:1 (effector:target), were able to eliminate tumor cells without SLL-peptide pre-loading (Figure 7G). As previously mentioned, to improve in a clinical perspective the safety of our transduced T cells, we included in the retroviral vector the iC9-suicide gene. In order to verify the capability of iC9 to induce apoptosis in transduced cells we perform functional experiments. Results demonstrated that also the second transgene is active, since iC9-SLL TCR T cells were promptly eliminated upon 24-hour exposure to 20 nM AP1903 (Figure 7C). The residual CD3+ V $\beta$ 1+ cells (average,  $6.3\% \pm 3.9\%$ ) still alive after 72 hours of AP1903 exposure were further expanded in culture with IL2, and tested for the presence of vector DNA, showing the absence of genetically modified T cells (Figure 7D).

**Figure 6**



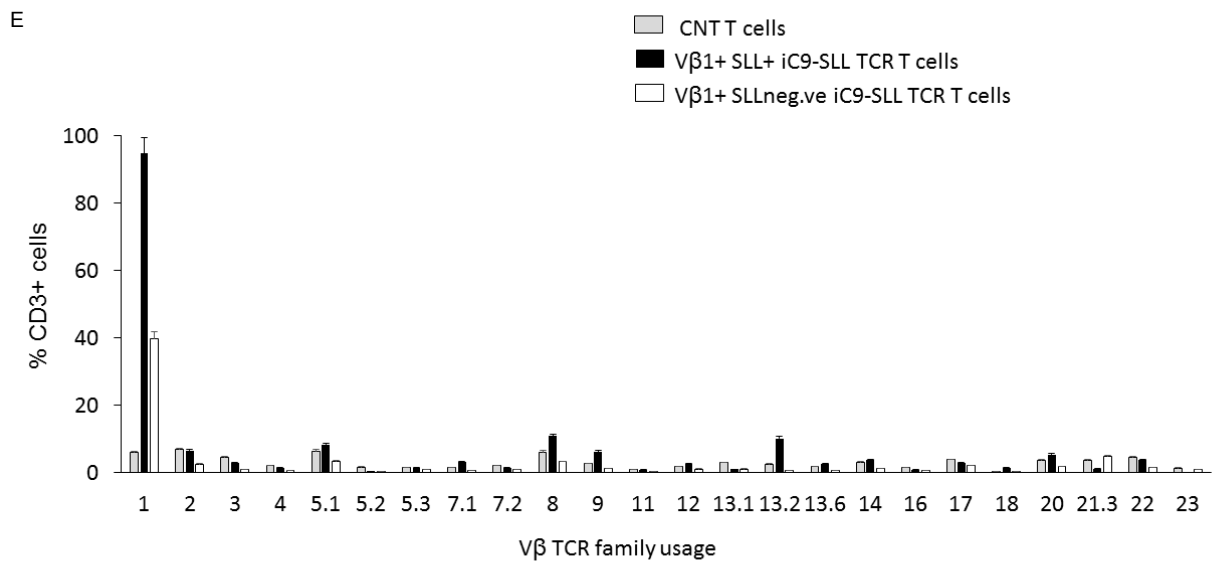


**Figure 6. Generation of iC9-SLL TCR T cells.** **A**,  $\alpha$  and  $\beta$  chains of SLL-PRAME TCR were cloned in frame with the suicide gene iC9 in a retroviral vector, with the separation of the transgenes through 2A sequences. **B**, Flow cytometry analyses in an esemplificative donor of untransduced (CNT T cells, top) or transduced with the retroviral vector iC9-SLL TCR (bottom) polyclonal T cells in vitro, activated through OKT3/CD28. TCR V $\beta$ 1 staining is shown in total CD3+, CD3+/CD4+, CD3+/CD8+ cells, whereas SLL-dextramer+ staining is shown in total CD3+ and in SLL-dextramer–sorted T cells (postsorting). **C**, The average of the positive TCR V $\beta$ 1 cells was shown in total CD3+, CD3+ CD8+, and CD3+ CD4+ T cells, whereas the average of positive SLL-dextramer cells was shown in CD3+ CD8+ and CD3+ CD4+ T cells. Data are expressed as average  $\pm$  SD from 8 healthy donors at day 15 of in vitro expansion. **D**, Fold expansion of untransduced T cell (CNT, gray dashed line) and iC9-SLL TCR T cell (black line), evaluated by Trypan blue count assay. Data represent results from 8 healthy donors. **E**, TCR-V $\beta$  repertoire analysis in iC9-SLL TCR T cells. TCR-V $\beta$  repertoire analysis showed no significant difference in TCR V $\beta$  usage between control T cells (CNT) and the transduced iC9-SLL TCR T cells (positive for V $\beta$ 1) subdivided in the T cell subset positive or negative for SLL tetramer staining.

**Figure 7**

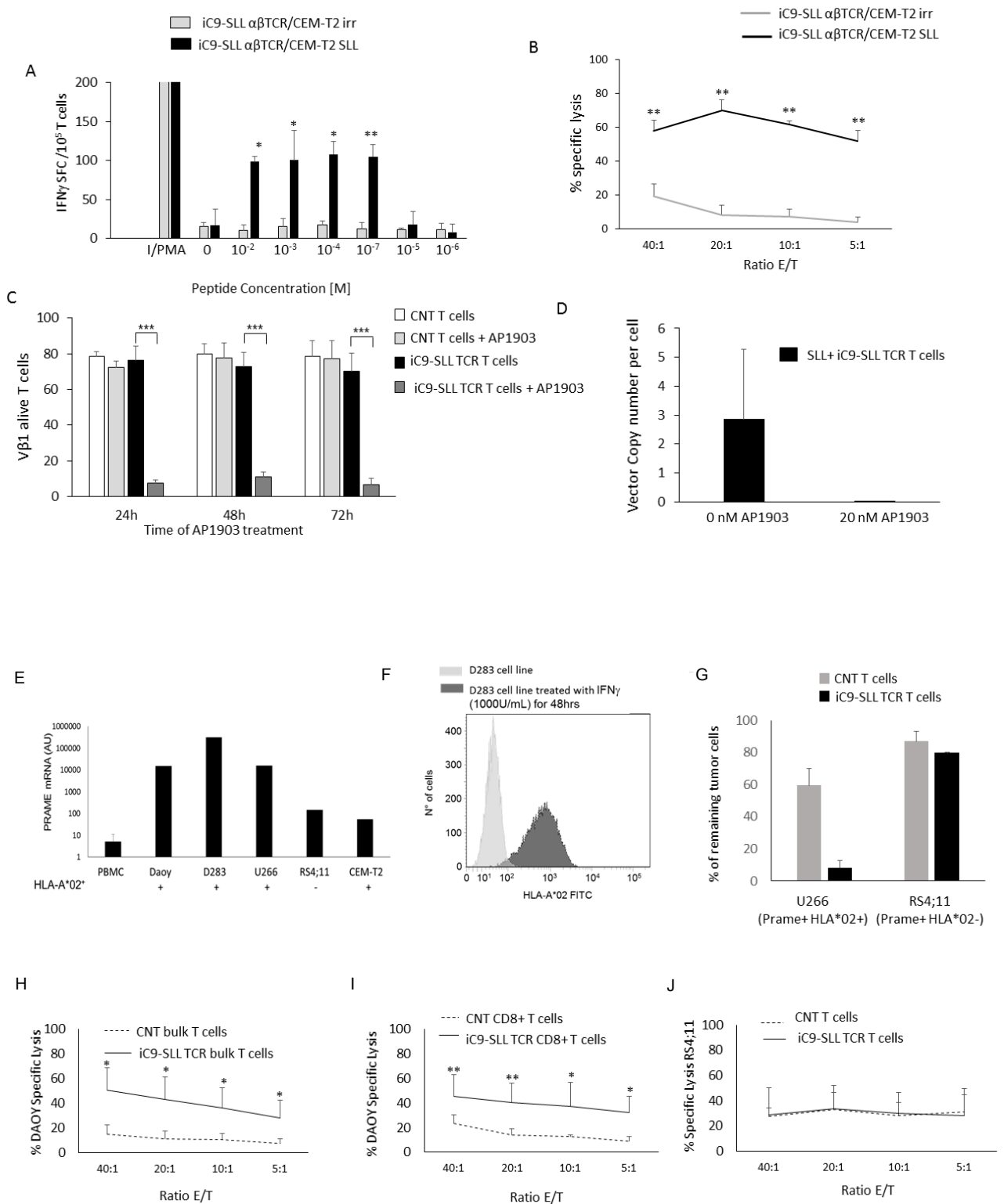


**Figure 7. A-D, In vitro functional analysis of iC9-SLL TCR T cells.** **A**, iC9-SLL TCR avidity assessed by IFN $\gamma$  ELISpot assays of CEM-T2 cell line loaded with an irrelevant peptide (gray bars) and the SLL-specific peptide (black bars). Ionomycin/phorbolmyristate acetate (I/PMA) was used as positive control. SFCs per 10<sup>5</sup> cells. Data represent the mean  $\pm$  SD of triplicate experiments. **B**, In vitro 51Cr release assay evaluating cytolytic activity of iC9-SLL TCR T cells on CEM-T2 tumor cell line loaded with an irrelevant (irr; gray line) or SLL-specific peptide (black line). **C**, Evaluation of percentage of alive (Annexin-V-/7AAD-) T cells grown in IL2 and exposed to 20 nmol/L AP1903 for 24, 48, or 72 hours. CD3+ TCR V $\beta$ 1+ T cells negative for Annexin-V/7AAD staining were considered to be alive after the activation of the iC9 suicide gene. Data from four healthy donors are expressed as average  $\pm$  SD. **D**, Analysis of the presence of retroviral vector sequence in iC9-SLL TCR T cells residual after AP1903 exposition. Quantitative PCR targeting specific retroviral sequence was carried out to establish whether V $\beta$ 1+ T cells residual after AP1903 exposition were genetically modified. Data from three independent experiments show that V $\beta$ 1p residual cells did not carry iC9-SLL TCR vector. **E-J, PRAME expression in tumor cell lines and in vitro functional analysis of iC9-SLL TCR T cells towards neoplastic cell lines.** **E**, Average of relative PRAME mRNA expression (AU) in 8 PBMC samples of adult healthy donors, MB cell lines DAOY (HLA-A\*02+), D283 (HLA-A\*02+, down-regulating HLA Class I molecule), Multiple Myeloma cell line U266 (HLA-A\*02+), Lymphoma cell line HDML2 (HLA-A\*02-), leukemia cell line RS4;11 (HLA-A\*02-), and lymphoblastoid cell line CEM-T2 (HLA-A\*02-). **F**, HLA-A\*02 expression in D283 cell line untreated (light gray histogram) and after treatment with IFN $\gamma$  (1000U/mL) for 48hrs (dark gray histogram). **G**, 7-days co-culture assay between effector cells [control CNT T cells (gray bars) or iC9-SLL TCR T cells (black bars)] and PRAME+ HLA-A\*02+ multiple myeloma U266 or PRAME+ HLA-A\*02- leukemia RS4;11 cell lines (1:1 Effector:target ratio). Data are expressed as average  $\pm$  SD from 3 donors. **H**, in vitro 51Cr release assay evaluating cytolytic activity of un-transduced (CNT) T cells (dotted line) and total CD3+ iC9-SLL TCR T cell (continuous line) vs DAOY cell line. **I**, in vitro 51Cr release assay evaluating cytolytic activity of CD8+ selected T cells un-transduced (CNT) (dotted line) or transduced with iC9-SLL TCR T cell (continuous line) vs HLA-A\*02+ DAOY cell line. **J**, in vitro 51Cr release assay evaluating cytolytic activity of un-transduced (CNT) T cells (dotted line) and total CD3+ iC9-SLL TCR T cell (continuous line) vs HLA-A02- RS4;11 cell line. n=3 replicates per point; representative of four donors. \* p-value= $\leq$ 0.05, \*\* p-value= $\leq$ 0.01, \*\*\* p-value= $\leq$ 0.001.

### **4.3. PRAME-specific TCR–redirected T cells exert antitumor activity toward HLA-A\*02-matched MB cell line**

The cytotoxic activity of iC9-SLL TCR T cells was also verified, by using standard 6-hour Cr<sup>51</sup> release assays, against the HLA-A\*02+ PRAME+ MB DAOY cell line and a negative control, namely the HLA-A\*02neg.ve PRAME+ RS4;11 cell line (Figure 7). We evidenced the greater lysis of HLA-A\*02+ PRAME+ MB cell line DAOY by iC9-SLL TCR T cells (43.3%±17.7% specific lysis at the E:T ratio of 20:1) than that observed with CNT T cells (11.3%±6.1%; p=0.004; Figure 7H). Otherwise, we performed functional experiments where we demonstrated no significant differences in cytotoxic activity between iC9-SLL TCR bulk T cells (Figure 7H) or iC9-SLL TCR CD8+ T cells (40.4%±15% specific lysis at the E:T ratio of 20:1) (Figure 7I). In addition, both transduced and control T cells showed negligible activity against the control target HLA-A\*02neg.ve PRAME+ RS4;11 cell line (Figure 7J), underlining the iC9-SLL TCR T cells specificity against the target. In longer-term assays, in which we co-cultured control or iC9-SLL TCR T cells with HLA-A\*02+ PRAME+ DAOY cells for 7 days, we found a significant reduction of DAOY tumor cells in the presence of iC9-SLL TCR T cells at E:T ratio of 1:1 (Figure 8A and 8B). To obtain similar results also on D283 cell line characterized by down-regulation of the HLA-A\*02 molecule (Figure 7F), we needed to pre-treat target cells with IFN $\gamma$  for 48 hours (Figure 8A). The efficacy of iC9-SLL TCR T cells against MB cell lines was confirmed by IFN- $\gamma$  production assessed by ELISA assays (Figure 8C). Moreover, we sought to evaluate whether SLL+ sorted T cells were still able to be functional towards HLA-A\*02+ PRAME+ DAOY cells. In particular, tumor control was mediated by the CD8+ V $\beta$ 1+ T cell subpopulation, whereas neither antigen-specific proliferation (Figure 9A and Figure 9B and 9C), nor a direct anti-tumor activity (Figure 8B), as well as cytokine production, evaluated in terms of IFN- $\gamma$  (Figure 9D), IL2 (Figure 9E) and TNF- $\alpha$  (Figure 9F), was observed when CD4+ V $\beta$ 1+ T cells were used as effector cells. In order to confirm our findings, we also decided to evaluate whether iC9-SLL TCR T cells were activated on primary HLA-A\*02+ MB cells derived from MB patient (#1). These cells were *in vitro* expanded until passage 5 and were confirmed to maintain both high PRAME expression (Figure 9G) and other neuronal markers, including



B3TUBB, S100A and GFAP. We observed a significant increase in IFN- $\gamma$  SFC T cells, when iC9-SLL TCR T cells were challenged with HLA-A\*02+ MB #1 cells, irrespectively of pre-treatment with IFN- $\gamma$ , with respect to the control condition (CNT T cells;  $p=0.004$ ). Negligible activity was valuated when iC9-SLL TCR T cells were stimulated in the presence of PRAME+ HLA-A\*02- MB #2 and #3 primary tumor cells (Figure 8D).

**Figure 8**

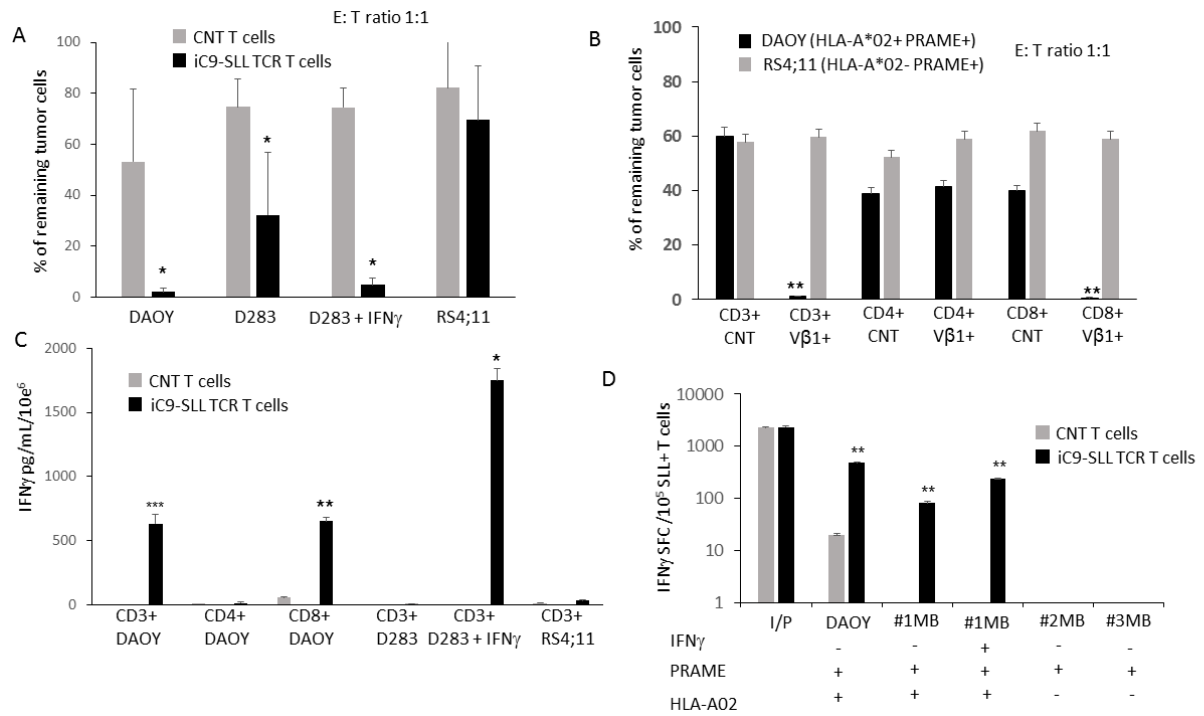
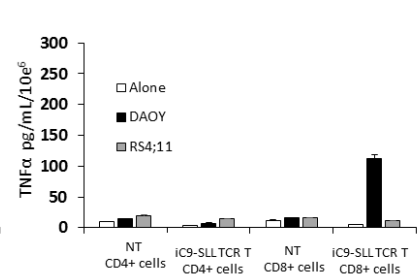
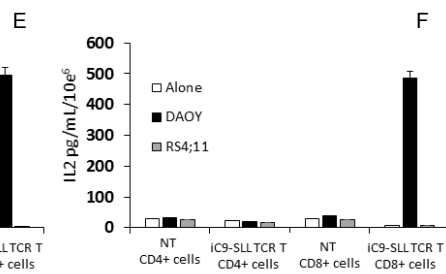
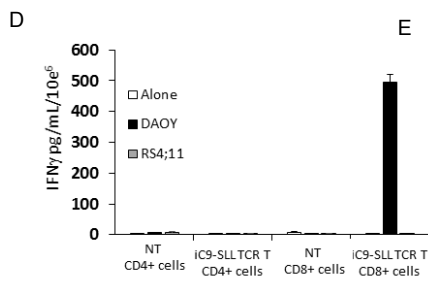
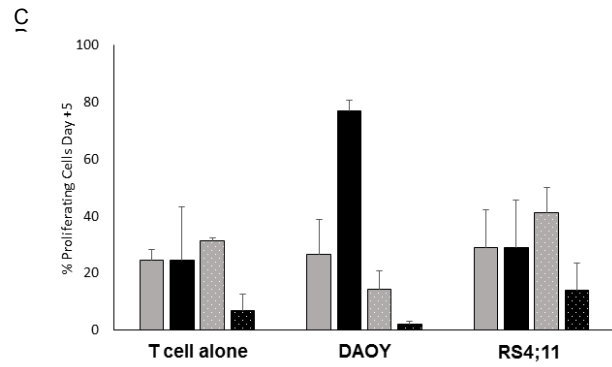
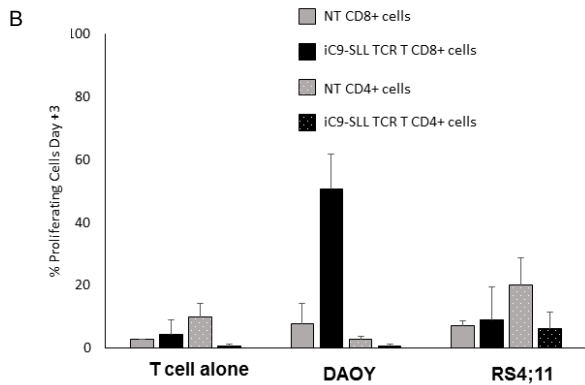
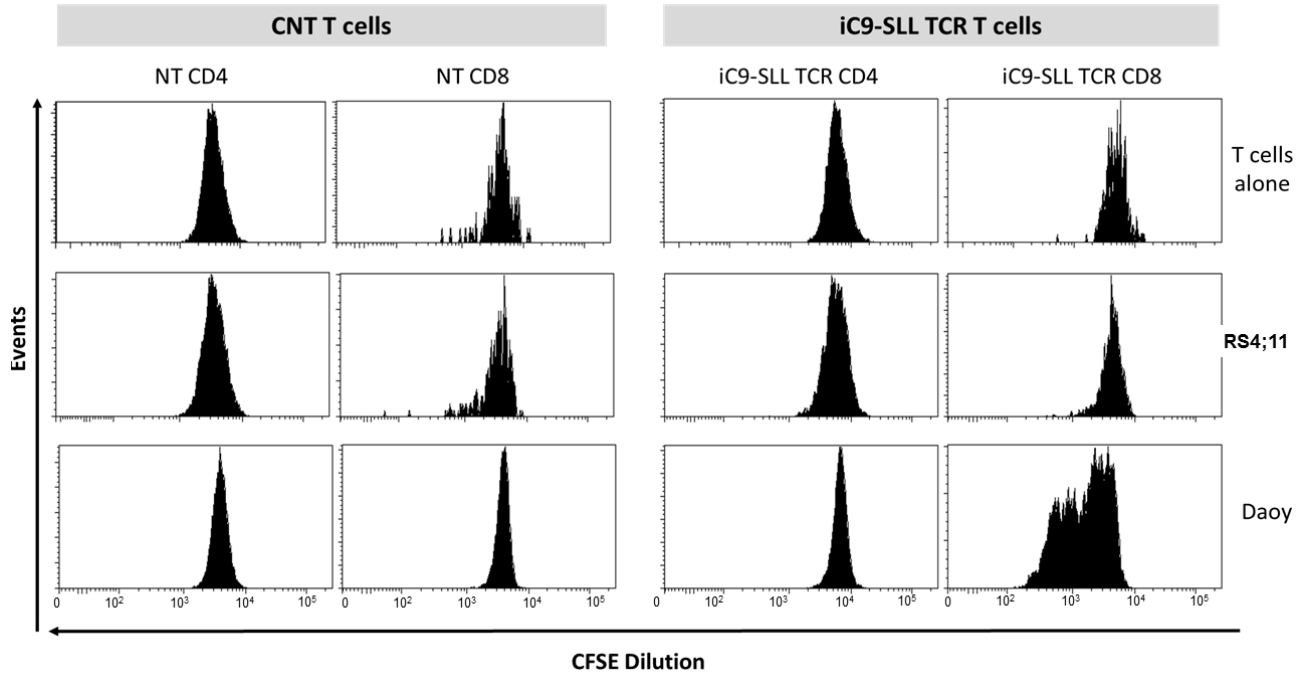


**Figure 8. Long-term in vitro functional analysis of iC9-SLL TCR T cells against MB cell lines and primary patient-derived tumor cells.** **A**, Seven-day co-culture assay between effector cells [control CNT T cells (gray bars) or iC9-SLL TCR T cells (black bars)] and PRAME+ HLA-A\*02+ MB cell line DAOY, PRAME+ MB cell line D283 down-regulating HLA Class I molecule, D283 cell line pretreated with IFN $\gamma$  (1,000 U/mL) for 48 hours, and PRAME+ HLA-A\*02- RS4;11 cell line (1:1 E:T ratio). Data are expressed as average  $\pm$  SD from three healthy donors. **B**, Seven-day co-culture assay (1:1 E:T ratio) between PRAME+ HLA-A\*02+ MB cell line DAOY (black bars) or PRAME+ HLA-A\*02- RS4;11 cell line (gray bars) and effector cells (control CNT T cells or V $\beta$ 1 $\beta$  iC9-SLL TCR T cells) sorted in the subset of CD3+, CD3+ CD4+, and CD3+ CD8+ T cells. Data are expressed as average  $\pm$  SD from three healthy donors. **C**, IFN $\gamma$  quantification by ELISA assay of supernatant after 24 hours of co-culture assay described in A and B. \* p-value=<0.05, \*\* p-value=<0.01, \*\*\* p-value=<0.001. **D**, IFN $\gamma$  ELISpot assays of un-transduced CNT T cells (gray bars) or iC9-SLL $\beta$  TCR T cells (black bars) challenged with primary MB cells derived from patient with PRAME+ HLA-A\*02+ (#1) with or w/out IFN $\gamma$  pretreatment, or patients with PRAME+ HLA-A\*02- (#2 and #3). SFCs per 10<sup>5</sup> cells. Data represent the average  $\pm$  SD of triplicate experiments (\* p-value=<0.05, \*\* p-value=<0.01).

**Figure 9**

A



G

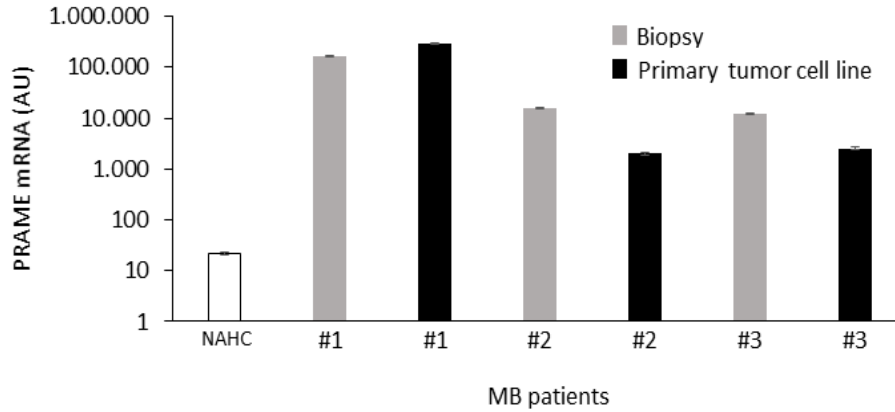


**Figure 9. A, proliferation analysis of  $V\beta 1^+$   $CD4^+$  and  $V\beta 1^+$   $CD8^+$  T cells exposed to HLA-A\*002+ PRAME+ cell line.**  $CD4^+$  and  $CD8^+$  CNT T cells or genetically modified with iC9-SLL TCR were analyzed for basal proliferation level (upper panels), 5 days of coculture with HLA-A\*002- PRAME+ cell line (RS4;11; middle panels) or HLA-A\*002+ PRAME+ DAOY cell line (lower panels). CFSE dilution was applied to visualize T cell proliferation. One representing donor is shown. **B-F, Functional analysis of  $V\beta 1^+$   $CD4^+$  and  $V\beta 1^+$   $CD8^+$  T cells exposed to HLA-A\*002+ PRAME+ MB cell line.**  $CD4^+$  (pointed color bars) and  $CD8^+$  (plain color bars) CNT T cells (gray bars) or genetically modified with iC9-SLL TCR (black bars) were analyzed for basal proliferation level, after coculture with HLA-A\*002- PRAME+ RS4;11 cell line or HLA-A\*002+ PRAME+ DAOY cell line (after three days in panel B, and 5 days in panel C). CFSE dilution was applied to visualize T cell proliferation. Data represent results from 3 HDs. **D-F,** cytokine analysis was performed upon 24 hrs of effector T cells cultured alone (white bars) or stimulated to HLA-A\*002+ PRAME+ DAOY cell line (black bars) or HLA-A\*002- PRAME+ RS4;11 cell line (gray bars).  $CD8^+$  but not  $CD4^+$  genetically modified with iC9-SLL TCR produced significant amount of  $IFN\gamma$  (D), IL2 (E) and  $TNF\alpha$  (F). **G,** Differential expression of PRAME mRNA between in vitro expanded primary cells (black bars) and the correspondent tumor biopsy (gray bar) of MB patient #1, #2 and #3.

#### **4.4. iC9-SLL TCR T cells exert antitumor activity *in vivo* in xenogeneic mouse models of MB.**

To strength our *in vitro* data, we performed *in vivo* antitumor experiments using iC9-SLL TCR+ T cells and xenogeneic NSG mouse models i.p. engrafted in Matrigel with a bulky MB tumor, represented by DAOY cells ( $2 \times 10^6$ ) genetically modified with firefly luciferase (FFLuc), to monitor tumor growth overtime by bioluminescent imaging (BLI) signal (Figure 10A). After establishment of bulky tumor (i.e. 20 days after DAOY i.p. injection), we treated mice with either control (CNT) or iC9-SLL TCR T cells (Figure 11A). On day 60 after T-cell infusion, 4 out of 5 mice treated with iC9-SLL TCR T cells had significantly better tumor control than mice receiving CNT T cells ( $6.4 \times 10^6 \pm 10 \times 10^6$  vs.  $11300 \times 10^6 \pm 8010 \times 10^6$  photons/second; respectively;  $p=0.03$ , Figure 11A and B). Then, in order to confirmed these evidence also in orthotopic MB mouse model, DAOY cells ( $2 \times 10^5$ ) are stereotaxically implanted into the cerebellum (Figure 10B and 10C). After 10 days, the mice were divided in three subgroups and each one received further stereotaxic surgery to infuse placebo (namely, no T cells;  $n=3$ ) or control T cells (namely, CNT T cells;  $n=6$ ) or T cells genetically modified with iC9-SLL TCR (namely, iC9-SLL TCR T cells;  $n=6$ ). On day +40, mice were sacrificed and cerebella surgically excised. By histopathologic analysis we evidenced that mice receiving iC9-SLL TCR T cells showed significantly lower tumor cell mass as compared to controls (2/6 vs 6/6, respectively). Tumor volume analysis (calculated along serial histologic brain sections as previously described) (118) displayed a significant reduction of the mass formed by DAOY tumor cells in iC9-SLL TCR T cells-treated mice as compared to controls (Figures 11C and D). We were also able to observe a significant reduction of the tumor volume when iC9-SLL TCR T cells were administered by intra-venous (i.v.) infusion (Figures 12A and B). To demonstrate that tumor control is a direct consequence of the T-cell migration across the blood brain barrier (BBB), we sacrificed mice and carried out anti-human CD3 IHC analysis on murine brain slides. Human T cells co-localized together with MB cells, while a negligible human T-cell infiltrate was seen in mouse brain sites not involved by the tumor (Figure 12C).

Since, pseudoprogression phenomena could represent a side effect in our system, we have studied the kinetics of tumor elimination when MB cell line (marked with FF-Luc) was intracranial implanted and T cells were injected i.v. In Figure 12D we

showed how tumor eradication was obtained in 15 days from T-cell infusion in the cohort of mice receiving iC9-SLL TCR T cells, this translating into a significant improvement of mice OS (Figure 12E). No neurological signs of toxicity was also recorded after iC9-SLL TCR T cell infusion, by applying comprehensive behavioural assessment involving a battery of 33 semi-quantitative tests for general health and sensory function, baseline behaviours and neurological reflexes.(114, 119)

To validate the IC9 safety system also in T cells infiltrating the cerebellum, we genetically modified iC9-SLL TCR T cells with a retroviral vector carrying the FireFly Luciferase to follow their *in vivo* elimination upon the i.p. administration of AP1903. As shown by Figure 6F, the systemic administration of the dimerizing drug allows a significant reduction of the BLI in the mouse cohort receiving iC9-SLL TCR T cells, but not in mice infused with CNT T cells. Moreover, anti-hCD3 IHC analysis on cerebella slides of mice treated with iC9-SLL TCR T cells shows that the administration of AP1903 completely eliminates tumor T-cell infiltration (Figure 10G).

**Figure 10**

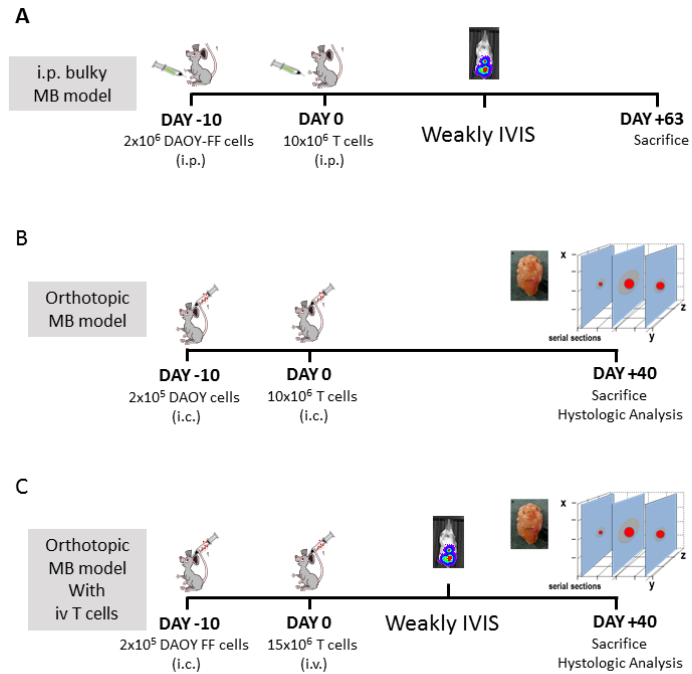


**Figure 10. Experimental plans of orthotopic xenograft mouse model for in vivo studies.** **A**, To measuring tumour control within a setting of bulky tumour, we performed in vivo i.p. model of MB. In particular, in NSG male mice of 5 weeks age, we engrafted i.p. 2x10<sup>6</sup> PRAME+ tumor cells (DAOY-FF-Luc.GFP) re-suspended in Matrigel. Ten days later, the mice received i.p. injection of 10<sup>7</sup> iC9-SLL TCR T cells or NT T cells. Tumor growth was evaluated weekly using IVIS imaging system until day of the sacrifice (Xenogen). **B**, DAOY cells (2 x10<sup>5</sup> per 5 µl) were stereotaxically implanted into the cerebellum of adult anesthetized female NSG mice. After 10 days following tumour implantation, the animals were stereotaxically infused (at the same co-ordinates of tumor implant) with placebo (PBS), un-transduced or iC9-SLL TCR T cells. After 4 weeks, animals were sacrificed and brains were evaluated for histopathologic H&E analysis to calculate tumor volume. **C**, T cells were inoculated i.v. into the tail vein of mice stereotaxically implanted with DAOY-FF-Luc.GFP. Mice were monitored with IVIS imaging system until tumor eradication, and then monitored for OS and toxicity signs.

**Figure 11**

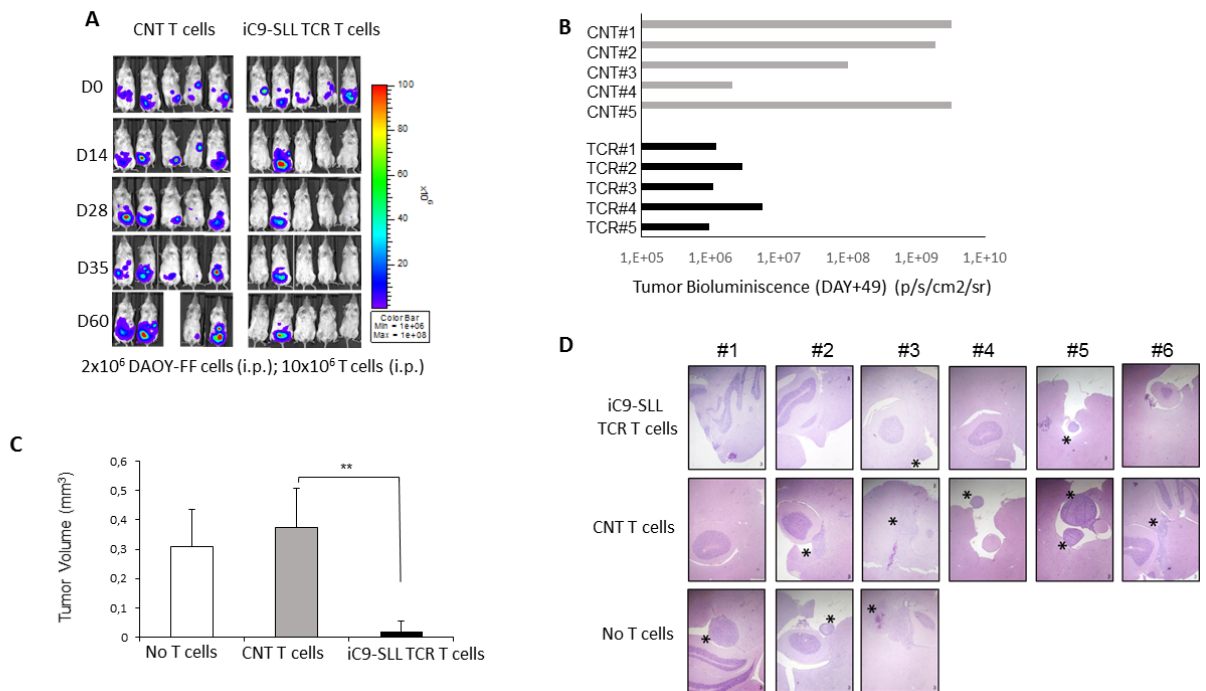


**Figure 11. iC9-SLL TCR T cells have in vivo antitumor activity against DAOY cell line.** **A and B,** Intraperitoneal administration of 2x10<sup>6</sup> DAOY-FFluc cells into NSG mice (n=10), followed by T-cell infusions [10<sup>7</sup>; 5 mice with untransduced (CNT) and 5 mice with iC9-SLL TCR T cells] and weekly BLI. BLI in individual mice from both treatment groups at day +49 from T-cell infusion is shown in **B**. Scale, 1x10<sup>6</sup> to 1x10<sup>8</sup> photons/second/cm2/sr. **C and D,** Stereotaxical administration of 2x10<sup>5</sup> DAOY cells into NSG mice (n=15), followed by intratumor infusions of placebo (PBS, No T cells; n=3), untransduced (CNT; n=6; 10<sup>7</sup>) or iC9-SLL TCR T cells (n=6; 10<sup>7</sup>). After 4 weeks, animals were sacrificed and brains were evaluated for histopathologic H&E analysis by serial section of the cerebellum. Tumor area (marked by asterisk where observed) of every slice was evaluated with a microscope, and average ± SD of tumor volumes is shown in **C**, whereas exemplificative slide section (magnification, x4) of the cerebella is shown in **D** (\* p-value=<0.05, \*\* p-value=<0.01).



**Figure 12**

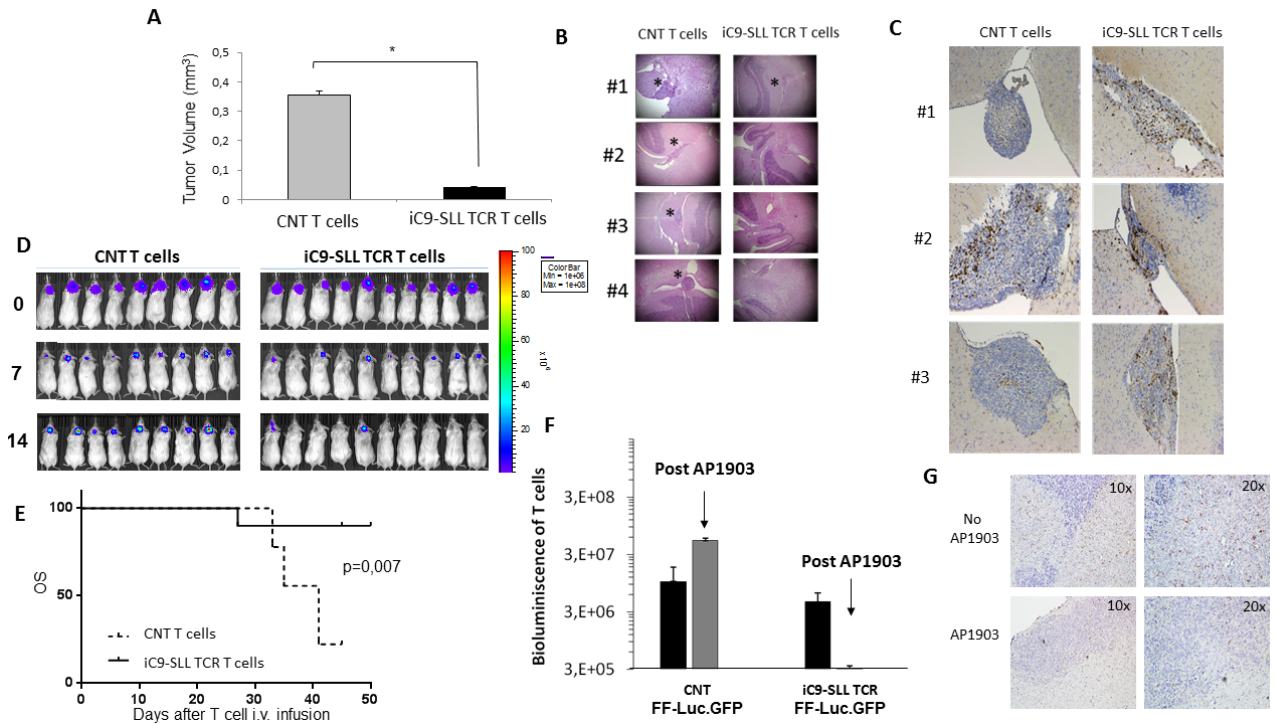


**Figure 12. iC9-SLL TCR T cells infused systemically have in vivo antitumor activity against orthotopic DAOY cell line implant.** **A–C**, Mice stereotactically implanted with DAOY were infused intravenously ( $n=8$ ) into the tail vein with untransduced (CNT;  $n=4$ ;  $10^7$ ) or iC9-SLL TCR T cells ( $n=4$ ;  $10^7$ ). Tumor area (marked by asterisk where observed) of every slice was evaluated with a microscope, and average  $\pm$  SD of tumor volumes is shown in **A**, whereas exemplificative slide section (magnification,  $\times 4$ ) of the cerebella is shown in **B**. **C**, Tumor T-cell infiltrates were analyzed by anti-hCD3 IHC on cerebella slides of mice sacrificed after 5 days from T-cell intravenous infusion. **D and E**, the dynamics of tumor regression after tail vein injection of untransduced (CNT;  $n=9$ ;  $10^7$ ) or iC9-SLL TCR T cells ( $n=9$ ;  $10^7$ ) was also evaluated, applying BLI in the orthotopic mouse model implanted with DAOY cell line genetically modified with FF-luc vector ( $n=18$ ) (**D**). **E**, After the tumor clearance (by 14 days after iC9-SLL TCR T-cell infusion), mice were evaluated for OS until day 45 (end of the experiment). **F and G**, Mice stereotactically implanted with WT DAOY were infused intravenously ( $n=8$ ) into the tail vein control (CNT;  $n=4$ ;  $10^7$ ) or dextramer-sorted iC9-SLL TCR T cells ( $n=4$ ;  $10^7$ ) also genetically modified with FF-Luc vector. At day +4 after T-cell infusion, all the mice were evaluated for BLI (black bars), and two mice in each cohort received intraperitoneal administration of 100 mg/mouse of the dimerizing AP1903 for two consecutive days. After additional 24 hours, all the mice were reevaluated for BLI (gray bars) and thereafter sacrificed. **G**, Tumor T-cell infiltrates were analyzed by anti-hCD3 IHC on cerebella slides of mice treated with iC9-SLL TCR T cells in the absence (top) or treated with AP1903 (bottom). The use of a systemically administration of AP1903 corresponded to a significant reduction of tumor T-cell infiltration.

## 5. Discussion

MB is the most common, highly aggressive, central nervous tumor of childhood and we have to improve the nowadays clinical protocols to obtain a better outcome for patients. MB is a solid tumor located in cerebellum and the development of new approaches is a big challenge for researchers. This study shows that adoptive immunotherapy with T cells redirected toward PRAME antigen could represent an innovative therapeutic tool for this neoplasm. CTAs such as PRAME could be a promising target for immunotherapy, those are normally not expressed in normal tissues (except the testis, which, however, has no expression of human leukocyte antigen molecules). (120) Several authors reported PRAME expression in many cancers, but the biological functions of PRAME expression in cancer is not yet completely elucidated due to the controversial association between PRAME expression and disease prognosis. (121-123) In particular, in solid malignancies, including head and neck cancer, (124,125) liposarcoma, (126) uveal melanoma, (127) osteosarcoma, (128,129) breast cancer (130) and neuroblastoma (131) high PRAME expression correlates with advanced stage disease and poor clinical outcome, whereas in pediatric acute leukemia PRAME overexpression was found to predict good outcome. (132,133) The expression of PRAME in MB has been previously evaluated and reported in gene expression datasets and publications (104,105) as having no correlation with patient clinical outcome. (105) We evaluated PRAME antigen expression levels in patients with MB and 82% of samples had PRAME mRNA expression levels higher than those of normal adult cerebellum. By applying a maximum-likelihood analysis statistical tool, we defined a PRAME expression cut-off able to subdivide patients into two categories, namely high (19 out of 51; 37%) and low PRAME- expressing patients. A low expression of PRAME correlated with a better 5-year OS probability, a finding similar to that observed in other cancers. (124,127,130,131) However, the correlation between better OS and low PRAME expression was evidenced in patients belonging to SHH- and G3-MB subgroups, while for WNT- and G4-MB subgroups this findings have to be confirmed extending patients' number. The statistically significant correlation between low PRAME expression and better OS probability was also maintained considering as cut-off for PRAME mRNA expression median value, as well as 1° and 3° quartiles.

Due to the high PRAME expression in most patients with MB and the protein presence in relapse samples, we can consider this CTA as a promising candidate for

targeted immunotherapies. Indeed, PRAME has already been evaluated, both *in vitro* (106,108) and *in vivo*, for its immunogenicity. It has been reported that PRAME induces CTL-mediated immune responses in melanoma and in acute/chronic leukemia, (134) and, thus, represents a promising target for TAA-specific immune therapies. Several vaccination trials have been recently exploited with this CTA as immunotarget, using full-length protein/peptides either alone or in combination with a different tumor antigen. In particular, PRAME-based immunotherapy had an acceptable safety profile and induced anti-PRAME-specific humoral and cellular immune responses in melanoma, (135,136) as well as in non-small cell lung cancer, (137) prostate carcinoma and renal clear cell carcinoma. (136)

However, data obtained by using PRAME as target in vaccination approaches, clearly evidenced the difficulty of *in vivo* reactivating PRAME-specific CD8<sup>+</sup> T cells, even after several consecutive rounds of administration of the immunogenic protein/peptides. Starting from this observation, we decided to validate PRAME relevance as target for adoptive TCR T-cell therapy with an alternative approach. Indeed, we genetically modified T cells in order to express a high-affinity TCR, specific for the PRAME-derived peptide SLL. This peptide is presented in the context of HLA-A\*02, which has a high worldwide frequency (i.e., 48.4% and 22.6% on average for Caucasian and Black ethnic groups, respectively). (138) Specifically, PRAME-specific TCR derived from the allogeneic HLA repertoire, was selected in view of its high avidity for the cognate peptide, high reactivity against several HLA-A\*02 positive PRAME-expressing tumor cell lines, as well as freshly isolated metastatic melanoma and primary leukemia cells. Anyway, genetically modified T cells were challenged against a large panel of non-malignant cells and no reactivity was reported, including either fresh or activated B cells, T cells, MØ1 and MØ2 macrophages, CD34 cells, immature dendritic cells (DCs) derived from either CD34<sup>+</sup> or CD14<sup>+</sup> cells. The T-cell clone from which SLL-TCR was derived exerted limited on-target reactivity against kidney epithelial cells and mature DC (mDC). However, the reactivity against the latter may be beneficial, since professional APCs like mDCs may contribute to enhance anti-tumor response and persistence of the infused T cells. (100) In the presented work, we chose to analyze the antitumor activity of PRAME-specific allo-TCR against MB cells. To increase the clinical safety of our modified PRAME-TCR product, the iC9 safety switch was introduced. In particular, iC9-SLL TCR T cells will be evaluated in an ongoing Phase I trial recruiting patients with either relapsed or refractory myeloid neoplasms (ClinicalTrials.gov Identifier NCT02743611).

Nowadays, iC9 is one of the most promising suicide genes for several reasons, including limited immunogenicity (139) and prompt activity, since more than 99% iC9-expressing T cells (iC9-T cells) are eliminated both *in vitro* and *in vivo* within 2 hours from the administration of a single dose of the prodrug AP1903 (Rimiducid, a synthetic and non-toxic ligand leading to iC9 dimerization and triggering of the apoptotic pathway). (139,140) Indeed, iC9 activation alone has been shown to produce rapid and sustained control of graft-versus-host disease caused by donor-derived iC9-T cells in recipients of allogeneic stem cell transplantation. (139-142)

To the best of our knowledge, data that shows the AP1903 possibility to reach the brain compartment and specifically eliminate genetically modified T cells through iC9 suicide gene induction doesn't exist. In this study, we have proved that the systemic administration of the dimerizing drug AP1903 in a MB orthotopic mouse model led to both BLI reduction in the total mouse body, including brain, and the lack of hCD3+ T cells in mouse cerebellum.

With the performed experiments, we actually proved that both transgenes in the construct (namely, SLL-TCR and iC9) are functionally active and iC9-SLL TCR T cells. Notably, the CD8+ T-cell subset, evidence a huge cytotoxic activity against DAOY cells, as well as D283 cells in which we re-established HLA expression by IFN- $\gamma$  treatment. IFNs have been used clinically to treat a variety of malignancies, protecting against disease by direct effects on target cells and by activating immune responses. (143,144) Our results support the possibility to use IFNs to trigger an adoptive T-cell therapy based on HLA-mediated target recognition. Fundamental for future prospective, despite the relevant difficulty to collect tumor material from patients with MB, we were able to challenge iC9-SLL TCR+ T cells with primary MB cells derived from the biopsy of one patient whose tumor cells were HLA-A\*02+ and PRAME+, and two patients characterized HLA-A\*02neg.ve and PRAME+ tumor cells, validating a significant PRAME specific T cell activation only in HLA-A\*02+ patient. A larger cohort of primary MB tissues need to be evaluated to strength this data.

The *in vitro* observations were also confirmed by *In vivo* animal models, evidencing that adoptive TCR T-cell therapy could be a new useful immunotherapy strategy to target MB cells. Notably, the *in vivo* experiments were performed without IFN $\gamma$  administration to obtain HLA upregulation. Moreover, a significant tumor control in the absence of undue toxicity was documented when both DAOY cells and iC9-SLL TCR T cells were injected through a stereotaxic approach in the mouse cerebellum. T cells were administered by i.v. infusion and demonstrated tumor control, coupled

with great T-cell infiltration of the tumour tissue and improved OS. No neurological sign of sufferance in the treated orthotropic mice was observed, proving that iC9-SLL TCR T cell activity was not associated to any side effect. These findings provide experimental support to the hypothesis that systemic administration of iC9-SLL TCR T cells could be a suitable and safe approach, particularly in view of T-cell migration across the BBB.

In conclusion, our work shows that iC9-SLL TCR T cells selectively kill MB cells, and might represent an innovative, effective strategy leading to a significant improvement of the outcome of MB patients. This novel form of immunotherapy should be tested in early phase clinical trials for MB patients with either relapsed or newly diagnosed disease, but with features predicting a high risk of treatment failure.

# References

1. Ostrom QT, Gittleman H, Fulop J, et al. CBTRUS statistical report: primary brain and central nervous system tumors diagnosed in the United States in 2008–2012. *Neuro Oncol* 2015; 17: 1–62.
2. Massimino M, Biassoni V, Gandola L, et al. Childhood medulloblastoma. *Crit Rev OncolHematol* 2016; 105: 35–51.
3. Even cancers want commitment: lineage identity and medulloblastoma formation. Eberhart CG. *Cancer Cell*. 2008 Aug 12; 14(2):105-7. doi: 10.1016/j.ccr.2008.07.011. PMID:18691544
4. Louis DN, Ohgaki H, Wiestler OD, et al. The 2007 WHO classification of tumours of the central nervous system. *Acta Neuropathol* 2007; 114: 97–109.
5. Louis DN, Perry A, Reifenberger G, et al. The 2016 World Health Organization classification of tumors of the central nervous system: a summary. *Acta Neuropathol* 2016; 131: 803–820.
6. Taylor MD, Northcott PA, Korshunov A, et al. Molecular subgroups of medulloblastoma: the current consensus. *Acta Neuropathol* 2012; 123: 465–472.
7. Northcott PA, Korshunov A, Witt H, et al. Medulloblastoma comprises four distinct molecular variants. *J Clin Oncol* 2011; 29: 1408–1414.
8. Shih DJ, Northcott PA, Remke M, et al. Cytogenetic prognostication within medulloblastoma subgroups. *J Clin Oncol* 2014; 32: 886–896.
9. Ramaswamy V, Remke M, Bouffet E, et al. Recurrence patterns across medulloblastoma subgroups: an integrated clinical and molecular analysis. *Lancet Oncol* 2013; 14: 1200–1207.
10. Cavalli FMG, Remke M, Rampasek L, et al. Intertumoral heterogeneity within medulloblastoma subgroups. *Cancer Cell* 2017; 31: 737–754.
11. Northcott PA, Buchhalter I, Morrissy AS, Hovestadt V, Weischenfeldt J, Ehrenberger T, et al.: The whole-genome landscape of medulloblastoma subtypes. *Nature* 547 : 311-317, 2017
12. Ellison DW, Dalton J, Kocak M, et al. Medulloblastoma: clinicopathological correlates of SHH, WNT, and non-SHH/WNT molecular subgroups. *Acta Neuropathol* 2011; 121: 381–396.
13. Kool M, Korshunov A, Remke M, et al. Molecular subgroups of medulloblastoma: an international meta-analysis of transcriptome, genetic aberrations, and clinical data of WNT, SHH, Group 3, and Group 4 medulloblastomas. *Acta Neuropathol* 2012; 123: 473–484.
14. Ellison DW, Onilude OE, Lindsey JC, et al. Beta-catenin status predicts a favorable outcome in childhood medulloblastoma: the United Kingdom Children’s Cancer Study

- Group Brain Tumour Committee. *J ClinOncol* 2005; 23: 7951–7957.
15. Di Giannatale A, Carai A, Cacchione A, et al. Anomalous vascularization in a Wntmedulloblastoma: a case report. *BMC Neurol* 2016; 16: 103.
  16. Zhukova N, Ramaswamy V, Remke M, et al. Subgroup-specific prognostic implications of TP53 mutation in medulloblastoma. *J ClinOncol* 2013; 31: 2927–2935.
  17. Northcott PA, Hielscher T, Dubuc A, et al. Pediatric and adult sonic hedgehog medulloblastoma are clinically and molecularly distinct. *ActaNeuropathol* 2011; 122: 231–240.
  18. Cho YJ, Tsherniak A, Tamayo P, et al. Integrative genomic analysis of medulloblastoma identifies a molecular subgroup that drives poor clinical outcome. *J ClinOncol* 2011; 29: 1424–1430.
  19. Kool M, Jones DT, Jäger N, et al. Genome sequencing of SHH medulloblastoma predicts genotype-related response to smoothed inhibition. *Cancer Cell* 2014; 25: 393–405.
  20. Robinson G, Parker M, Kranenburg TA, et al. Novel mutations target distinct subgroups of medulloblastoma. *Nature* 2012; 488: 43–48.
  21. Fujii K and Miyashita T. Gorlin syndrome (nevoid basal cell carcinoma syndrome): update and literature review. *PediatrInt* 2014; 56: 667–674.
  22. Miele E, Mastronuzzi A, Po A, et al. Characterization of medulloblastoma in Fanconi anemia: a novel mutation in the BRCA2 gene and SHH molecular subgroup. *Biomark Res* 2015; 3: 13.
  23. Kawauchi D, Robinson G, Uziel T, et al. A mouse model of the most aggressive subgroup of human medulloblastoma. *Cancer Cell* 2012; 21: 168–180.
  24. Moavero R, Folgiero V, Carai A, et al. Metastatic group 3 medulloblastoma in a patient with tuberous sclerosis complex: case description and molecular characterization of the tumor. *Pediatr Blood Cancer* 2016; 63: 719–722.
  25. Jones DT, Jäger N, Kool M, et al. Dissecting the genomic complexity underlying medulloblastoma. *Nature* 2012; 488: 100–105.
  26. Shih DJ, Northcott PA, Remke M, et al. Cytogenetic prognostication within medulloblastoma subgroups. *J ClinOncol* 2014; 32: 886–896.
  27. Claudia Miranda Kuzan-Fischer, Kyle Juraschka, and Michael D. Taylor. Medulloblastoma in the Molecular Era. *J Korean Neurosurg Soc.* 2018 May; 61(3): 292–301.
  28. Ribic K1, Relly C, Landolt MA, et al. Outcome of medulloblastoma in children: long-term complications and quality of life. *Neuropediatrics.* 2005 Dec;36(6):357-65.
  29. Gopalakrishnan CV, Dhakoji A, Menon G, et al. Factors Predicting the Need for Cerebrospinal Fluid Diversion Following Posterior Fossa Tumor Surgery in Children. *Pediatric Neurosurgery.* 2012; 48(2):93–101. [PubMed: 23038047]
  30. Robertson PL, Muraszko KM, Holmes EJ, et al. Incidence and Severity of Postoperative

- Cerebellar Mutism Syndrome in Children with Medulloblastoma: a Prospective Study by the Children's Oncology Group. *Journal of Neurosurgery: Pediatrics*. 2006; 105:444–451. [PubMed: 17184075] [The only prospective study on cerebellar mutism.]
31. Packer RJ, Gajjar A, Vezina G, et al. Phase III Study of Craniospinal Radiation Therapy Followed by Adjuvant Chemotherapy for Newly Diagnosed Average-Risk Medulloblastoma. *Journal of Clinical Oncology*. 2006; 24(25):4202–4208. [PubMed: 16943538] [Even though this is an older study it provides the backbone for current standard risk therapy in medulloblastoma. Due to smaller sample sizes pediatric trials are slower to complete.]
  32. Kortman RD, Kuhl J, Timmerman B, et al. Postoperative Neoadjuvant Chemotherapy Before Radiotherapy as Compared to Immediate Radiotherapy Followed by Maintenance Chemotherapy in the Treatment of Medulloblastoma in Childhood: Results of the German Prospective Randomized Trial HIT '91. *International Journal of Radiation Oncology Biology Physics*. 2000; 46(2):269–279.
  33. Von Hoff DD, Schilsky R, Reichert CM, et al. Toxic effects of cis-dichlorodiammineplatinum(II) in Man. *Cancer Treatment Reports*. 1979; 63:1527–31. [PubMed: 387223]
  34. Rowinsky EK, Donehower RC. The Clinical Pharmacology and Use of Antimicrotubule Agents in Cancer Chemotherapeutics. *Pharmacology and Therapeutics*. 1991; 52:35–84. [PubMed: 1687171]
  35. Fruh, K.; Picker, L. CD8+ T cell programming by cytomegalovirus vectors: Applications in prophylactic and therapeutic vaccination. *Curr. Opin. Immunol*. 2017, 47, 52–56.
  36. Kreiter, S.; Vormehr, M.; van de Roemer, N.; Diken, M.; Lower, M.; Diekmann, J.; Boegel, S.; Schrors, B.; Vascotto, F.; Castle, J.C.; et al. Mutant MHC class II epitopes drive therapeutic immune responses to cancer. *Nature* 2015, 520, 692–696.
  37. Sampson, J.H.; Heimberger, A.B.; Archer, G.E.; Aldape, K.D.; Friedman, A.H.; Friedman, H.S.; Gilbert, M.R.; Herndon, J.E., II; McLendon, R.E.; Mitchell, D.A.; et al. Immunologic escape after prolonged progression-free survival with epidermal growth factor receptor variant III peptide vaccination in patients with newly diagnosed glioblastoma. *J. Clin. Oncol*. 2010, 28, 4722–4729.
  38. Sampson, J.H.; Maus, M.V.; June, C.H. Immunotherapy for Brain Tumors. *J. Clin. Oncol*. 2017, 35, 2450–2456.
  39. Schlager, C.; Korner, H.; Krueger, M.; Vidoli, S.; Haberl, M.; Mielke, D.; Brylla, E.; Issekutz, T.; Cabanas, C.; Nelson, P.J.; et al. Effector T-cell trafficking between the leptomeninges and the cerebrospinal fluid. *Nature* 2016, 530, 349–353.



40. Aspelund, A.; Antila, S.; Proulx, S.T.; Karlsen, T.V.; Karaman, S.; Detmar, M.; Wiig, H.; Alitalo, K. A dural lymphatic vascular system that drains brain interstitial fluid and macromolecules. *J. Exp. Med.* 2015, 212, 991–999.
41. Louveau, A.; Smirnov, I.; Keyes, T.J.; Eccles, J.D.; Rouhani, S.J.; Peske, J.D.; Derecki, N.C.; Castle, D.; Mandell, J.W.; Lee, K.S.; et al. Structural and functional features of central nervous system lymphatic vessels. *Nature* 2015, 523, 337–341.
42. Haubner, F.; Ohmann, E.; Pohl, F.; Strutz, J.; Gassner, H.G. Wound healing after radiation therapy: Review of the literature. *Radiat. Oncol.* 2012, 7, 162.
43. Liu, H.; Li, B.; Jia, X.; Ma, Y.; Gu, Y.; Zhang, P.; Wei, Q.; Cai, J.; Cui, J.; Gao, F.; et al. Radiation-induced decrease of CD8<sup>+</sup> dendritic cells contributes to Th1/Th2 shift. *Int. Immunopharmacol.* 2017, 46, 178–185.
44. Vandenabeele, P.; Vandecasteele, K.; Bachert, C.; Krysko, O.; Krysko, D.V. Immunogenic Apoptotic Cell Death and Anticancer Immunity. *Adv. Exp. Med. Biol.* 2016, 930, 133–149.
45. Dunkel, I.J.; Gardner, S.L.; Garvin, J.H., Jr.; Goldman, S.; Shi, W.; Finlay, J.L. High-dose carboplatin, thiotepa, and etoposide with autologous stem cell rescue for patients with previously irradiated recurrent medulloblastoma. *Neuro-Oncology* 2010, 12, 297–303.
46. Welters, M.J.; van der Sluis, T.C.; van Meir, H.; Loof, N.M.; van Ham, V.J.; van Duikeren, S.; Santegoets, S.J.; Arens, R.; de Kam, M.L.; Cohen, A.F.; et al. Vaccination during myeloid cell depletion by cancer chemotherapy fosters robust T cell responses. *Sci. Transl. Med.* 2016, 8, 334ra352.
47. Gattinoni, L.; Finkelstein, S.E.; Klebanoff, C.A.; Antony, P.A.; Palmer, D.C.; Spiess, P.J.; Hwang, L.N.; Yu, Z.; Wrzesinski, C.; Heimann, D.M.; et al. Removal of homeostatic cytokine sinks by lymphodepletion enhances the efficacy of adoptively transferred tumor-specific CD8<sup>+</sup> T cells. *J. Exp. Med.* 2005, 202, 907–912.
48. Sanchez-Perez, L.A.; Choi, B.D.; Archer, G.E.; Cui, X.; Flores, C.; Johnson, L.A.; Schmittling, R.J.; Snyder, D.; Herndon, J.E., II; Bigner, D.D.; et al. Myeloablativetemozolomide enhances CD8(+) T-cell responses to vaccine and is required for efficacy against brain tumors in mice. *PLoS ONE* 2013, 8, e59082.
49. Mitchell, D.A.; Cui, X.; Schmittling, R.J.; Sanchez-Perez, L.; Snyder, D.J.; Congdon, K.L.; Archer, G.E.; Desjardins, A.; Friedman, A.H.; Friedman, H.S.; et al. Monoclonal antibody blockade of IL-2 receptor alpha during lymphopenia selectively depletes regulatory T cells

- in mice and humans. *Blood* 2011, 118, 3003–3012.
50. Mitchell, D.A.; Batich, K.A.; Gunn, M.D.; Huang, M.N.; Sanchez-Perez, L.; Nair, S.K.; Congdon, K.L.; Reap, E.A.; Archer, G.E.; Desjardins, A.; et al. Tetanus toxoid and CCL3 improve dendritic cell vaccines in mice and glioblastoma patients. *Nature* 2015, 519, 366–369.
  51. Batich, K.A.; Swartz, A.M.; Sampson, J.H. Preconditioning Vaccine Sites for mRNA-Transfected Dendritic Cell Therapy and Antitumor Efficacy. *Methods mol. Biol.* 2016, 1403, 819–838.
  52. Hao, C.; Tian, J.; Liu, H.; Li, F.; Niu, H.; Zhu, B. Efficacy and safety of anti-PD-1 and anti-PD-1 combined with anti-CTLA-4 immunotherapy to advanced melanoma: A systematic review and meta-analysis of randomized controlled trials. *Medicine* 2017, 96, e7325.
  53. Alizadeh, A.A.; Aranda, V.; Bardelli, A.; Blanpain, C.; Bock, C.; Borowski, C.; Caldas, C.; Califano, A.; Doherty, M.; Elsner, M.; et al. Toward understanding and exploiting tumor heterogeneity. *Nat. Med.* 2015, 21, 846–853.
  54. Alexandrov, L.B.; Nik-Zainal, S.; Wedge, D.C.; Aparicio, S.A.; Behjati, S.; Biankin, A.V.; Bignell, G.R.; Bolli, N.; Borg, A.; Borresen-Dale, A.L.; et al. Signatures of mutational processes in human cancer. *Nature* 2013, 500, 415–421.
  55. Fontebasso, A.M.; Gayden, T.; Nikbakht, H.; Neirinck, M.; Papillon-Cavanagh, S.; Majewski, J.; Jabado, N. Epigenetic dysregulation: A novel pathway of oncogenesis in pediatric brain tumors. *ActaNeuropathol.* 2014, 128, 615–627.
  56. Koebel, C.M.; Vermi, W.; Swann, J.B.; Zerafa, N.; Rodig, S.J.; Old, L.J.; Smyth, M.J.; Schreiber, R.D. Adaptive immunity maintains occult cancer in an equilibrium state. *Nature* 2007, 450, 903–907.
  57. Kozłowska, A.; Mackiewicz, J.; Mackiewicz, A. Therapeutic gene modified cell based cancer vaccines. *Gene* 2013, 525, 200–207.
  58. Klepsch, V.; Hermann-Kleiter, N.; Baier, G. Beyond CTLA-4 and PD-1: Orphan nuclear receptor NR2F6 as T cell signaling switch and emerging target in cancer immunotherapy. *Immunol. Lett.* 2016, 178, 31–36.
  59. Lob, S.; Konigsrainer, A.; Rammensee, H.G.; Opelz, G.; Terness, P. Inhibitors of indoleamine-2,3-dioxygenase for cancer therapy: Can we see the wood for the trees? *Nat. Rev. Cancer* 2009, 9, 445–452.

60. Gabrilovich, D.I.; Ostrand-Rosenberg, S.; Bronte, V. Coordinated regulation of myeloid cells by tumours. *Nat. Rev. Immunol.* 2012, 12, 253–268.
61. Duraiswamy, J.; Kaluza, K.M.; Freeman, G.J.; Coukos, G. Dual blockade of PD-1 and CTLA-4 combined with tumor vaccine effectively restores T-cell rejection function in tumors. *Cancer Res.* 2013, 73, 3591–3603.
62. Borghaei, H.; Paz-Ares, L.; Horn, L.; Spigel, D.R.; Steins, M.; Ready, N.E.; Chow, L.Q.; Vokes, E.E.; Felip, E.; Holgado, E.; et al. Nivolumab versus Docetaxel in Advanced Nonsquamous Non-Small-Cell Lung Cancer. *N. Engl. J. Med.* 2015, 373, 1627–1639.
63. Baumann, B.C.; Kao, G.D.; Mahmud, A.; Harada, T.; Swift, J.; Chapman, C.; Xu, X.; Discher, D.E.; Dorsey, J.F. Enhancing the efficacy of drug-loaded nanocarriers against brain tumors by targeted radiation therapy. *Oncotarget* 2013, 4, 64–79.
64. Sattiraju, A.; Xiong, X.; Pandya, D.N.; Wadas, T.J.; Xuan, A.; Sun, Y.; Jung, Y.; Solingapuram Sai, K.K.; Dorsey, J.F.; Li, K.C.; et al. Alpha particle enhanced Blood Brain/Tumor Barrier permeabilization in glioblastomas using integrin alpha-v beta-3 targeted liposomes. *Mol. Cancer Ther.* 2017.
65. Gholamin, S.; Mitra, S.S.; Feroze, A.H.; Liu, J.; Kahn, S.A.; Zhang, M.; Esparza, R.; Richard, C.; Ramaswamy, V.; Remke, M.; et al. Disrupting the CD47-SIRPalpha anti-phagocytic axis by a humanized anti-CD47 antibody is an efficacious treatment for malignant pediatric brain tumors. *Sci. Transl. Med.* 2017, 9, eaaf2968.
66. Hwang, S.L.; Chung, N.P.; Chan, J.K.; Lin, C.L. Indoleamine 2,3-dioxygenase (IDO) is essential for dendritic cell activation and chemotactic responsiveness to chemokines. *Cell Res.* 2005, 15, 167–175.
67. Mbongue, J.C.; Nicholas, D.A.; Torrez, T.W.; Kim, N.S.; Firek, A.F.; Langridge, W.H. The Role of Indoleamine 2,3-Dioxygenase in Immune Suppression and Autoimmunity. *Vaccines* 2015, 3, 703–729.
68. Wainwright, D.A.; Balyasnikova, I.V.; Chang, A.L.; Ahmed, A.U.; Moon, K.S.; Auffinger, B.; Tobias, A.L.; Han, Y.; Lesniak, M.S. IDO expression in brain tumors increases the recruitment of regulatory T cells and negatively impacts survival. *Clin. Cancer Res.* 2012, 18, 6110–6121.
69. Jahnisch, H.; Fussel, S.; Kiessling, A.; Wehner, R.; Zastrow, S.; Bachmann, M.; Rieber, E.P.; Wirth, M.P.; Schmitz, M. Dendritic cell-based immunotherapy for prostate cancer.

Clin. Dev. Immunol. 2010, 2010, 517493.

70. Pollack, I.F.; Jakacki, R.I.; Butterfield, L.H.; Hamilton, R.L.; Panigrahy, A.; Potter, D.M.; Connelly, A.K.; Dibridge, S.A.; Whiteside, T.L.; Okada, H. Antigen-specific immune responses and clinical outcome after vaccination with glioma-associated antigen peptides and polyinosinic-polycytidylic acid stabilized by lysine and carboxymethylcellulose in children with newly diagnosed malignant brainstem and nonbrainstem gliomas. *J. Clin. Oncol.* 2014, 32, 2050–2058.
71. Holtkamp, S.; Kreiter, S.; Selmi, A.; Simon, P.; Koslowski, M.; Huber, C.; Tureci, O.; Sahin, U. Modification of antigen-encoding RNA increases stability, translational efficacy, and T-cell stimulatory capacity of dendritic cells. *Blood* 2006, 108, 4009–4017.
72. Kranz, L.M.; Diken, M.; Haas, H.; Kreiter, S.; Loquai, C.; Reuter, K.C.; Meng, M.; Fritz, D.; Vascotto, F.; Hefesha, H.; et al. Systemic RNA delivery to dendritic cells exploits antiviral defence for cancer immunotherapy. *Nature* 2016, 534, 396–401.
73. Kreiter, S.; Selmi, A.; Diken, M.; Koslowski, M.; Britten, C.M.; Huber, C.; Tureci, O.; Sahin, U. Intranodal vaccination with naked antigen-encoding RNA elicits potent prophylactic and therapeutic antitumoral immunity. *Cancer Res.* 2010, 70, 9031–9040.
74. Coban, C.; Kobiyama, K.; Aoshi, T.; Takeshita, F.; Horii, T.; Akira, S.; Ishii, K.J. Novel strategies to improve DNA vaccine immunogenicity. *Curr. Gene Ther.* 2011, 11, 479–484.
75. Aurelian, L. Oncolytic viruses as immunotherapy: Progress and remaining challenges. *OncoTargetsTher.* 2016, 9, 2627–2637.
76. Kaufman, H.L.; Kohlhapp, F.J.; Zloza, A. Oncolytic viruses: A new class of immunotherapy drugs. *Nat. Rev. Drug Discov.* 2015, 14, 642–662.
77. Killock, D. Skin cancer: T-VEC oncolytic viral therapy shows promise in melanoma. *Nat. Rev. Clin. Oncol.* 2015, 12, 438.
78. Kohlhapp, F.J.; Kaufman, H.L. Molecular Pathways: Mechanism of Action for TalimogeneLaherpaprevic, a New Oncolytic Virus Immunotherapy. *Clin. Cancer Res.* 2016, 22, 1048–1054.
79. Yu, Y.A.; Galanis, C.; Woo, Y.; Chen, N.; Zhang, Q.; Fong, Y.; Szalay, A.A. Regression of human pancreatic tumor xenografts in mice after a single systemic injection of recombinant vaccinia virus GLV-1h68. *Mol. Cancer Ther.* 2009, 8, 141–151.

80. Saha, D.; Martuza, R.L.; Rabkin, S.D. Macrophage Polarization Contributes to Glioblastoma Eradication by Combination Immunovirotherapy and Immune Checkpoint Blockade. *Cancer Cell* 2017, 32, 253–267.
81. Garfall, A.L.; Maus, M.V.; Hwang, W.T.; Lacey, S.F.; Mahnke, Y.D.; Melenhorst, J.J.; Zheng, Z.; Vogl, D.T.; Cohen, A.D.; Weiss, B.M.; et al. Chimeric Antigen Receptor T Cells against CD19 for Multiple Myeloma. *N. Engl. J. Med.* 2015, 373, 1040–1047.
82. Grupp, S.A.; Kalos, M.; Barrett, D.; Aplenc, R.; Porter, D.L.; Rheingold, S.R.; Teachey, D.T.; Chew, A.; Hauck, B.; Wright, J.F.; et al. Chimeric antigen receptor-modified T cells for acute lymphoid leukemia. *N. Engl. J. Med.* 2013, 368, 1509–1518.
83. Kalos, M.; Levine, B.L.; Porter, D.L.; Katz, S.; Grupp, S.A.; Bagg, A.; June, C.H. T cells with chimeric antigen receptors have potent antitumor effects and can establish memory in patients with advanced leukemia. *Sci. Transl. Med.* 2011, 3, 95ra73.
84. Louis, C.U.; Savoldo, B.; Dotti, G.; Pule, M.; Yvon, E.; Myers, G.D.; Rossig, C.; Russell, H.V.; Diouf, O.; Liu, E.; et al. Antitumor activity and long-term fate of chimeric antigen receptor-positive T cells in patients with neuroblastoma. *Blood* 2011, 118, 6050–6056.
85. Maude, S.L.; Frey, N.; Shaw, P.A.; Aplenc, R.; Barrett, D.M.; Bunin, N.J.; Chew, A.; Gonzalez, V.E.; Zheng, Z.; Lacey, S.F.; et al. Chimeric antigen receptor T cells for sustained remissions in leukemia. *N. Engl. J. Med.* 2014, 371, 1507–1517.
86. Porter, D.L.; Hwang, W.T.; Frey, N.V.; Lacey, S.F.; Shaw, P.A.; Loren, A.W.; Bagg, A.; Marcucci, K.T.; Shen, A.; Gonzalez, V.; et al. Chimeric antigen receptor T cells persist and induce sustained remissions in relapsed refractory chronic lymphocytic leukemia. *Sci. Transl. Med.* 2015, 7, 303ra139.
87. Brown, C.E.; Alizadeh, D.; Starr, R.; Weng, L.; Wagner, J.R.; Naranjo, A.; Ostberg, J.R.; Blanchard, M.S.; Kilpatrick, J.; Simpson, J.; et al. Regression of Glioblastoma after Chimeric Antigen Receptor T-Cell Therapy. *N. Engl. J. Med.* 2016, 375, 2561–2569.
88. Ahmed, N.; Brawley, V.; Hegde, M.; Bielałowicz, K.; Kalra, M.; Landi, D.; Robertson, C.; Gray, T.L.; Diouf, O.; Wakefield, A.; et al. HER2-Specific Chimeric Antigen Receptor-Modified Virus-Specific T Cells for Progressive Glioblastoma: A Phase 1 Dose-Escalation Trial. *JAMA Oncol.* 2017, 3, 1094–1101.
89. Hegde, M.; Mukherjee, M.; Grada, Z.; Pignata, A.; Landi, D.; Navai, S.A.; Wakefield, A.; Fousek, K.; Bielałowicz, K.; Chow, K.K.; et al. Tandem CAR T cells targeting HER2 and

- IL13Ralpha2 mitigate tumor antigen escape. *J. Clin. Investig.* 2016, 126, 3036–3052.
90. Di Rosa, M.; Sanfilippo, C.; Libra, M.; Musumeci, G.; Malaguarnera, L. Different pediatric brain tumors are associated with different gene expression profiling. *ActaHistochem.* 2015, 117, 477–485.
  91. Topalian, S.L.; Hodi, F.S.; Brahmer, J.R.; Gettinger, S.N.; Smith, D.C.; McDermott, D.F.; Powderly, J.D.; Carvajal, R.D.; Sosman, J.A.; Atkins, M.B.; et al. Safety, activity, and immune correlates of anti-PD-1 antibody in cancer. *N. Engl. J. Med.* 2012, 366, 2443–2454.
  92. Christopher R Showers Adam M Sonabend, Richard CE Anderson (2014) Immunopathology of Central Nervous System Tumors. *Immunome Res* 10:077. doi: 10.4172/1745-7580.1000077
  93. Kasuga C, Nakahara Y, Ueda S, Hawkins C, Taylor MD, Smith CA, Rutka JT (2008) Expression of MAGE and GAGE genes in medulloblastoma and modulation of resistance to chemotherapy. *Laboratory investigation. J NeurosurgPediatr* 1:305–313
  94. Oba-Shinjo SM, Caballero OL, Jungbluth AA, Rosemberg S, Old LJ, Simpson AJ, Marie SK (2008) Cancer-testis (CT) antigen expression in medulloblastoma. *Cancer Immun* 8:7
  95. Scanlan MJ, Gure AO, Jungbluth AA, et al. (2002b). Cancer/testis antigens: An expanding family of targets for cancer immunotherapy. *Immunol Rev*, 188, 22–32.
  96. Caballero OL, Chen YT. (2009a). Cancer/testis (CT) antigens: Potential targets for immunotherapy. *Cancer Sci*, 100, 2014–2021.
  97. Ghafouri-Fard S, Modarressi M-H. (2009). Cancer-testis antigens: Potential targets for cancer immunotherapy. *Arch Iran Med*, 12, 395–404.
  98. Grigoriadis A, Caballero OL, Hoek KS, et al. (2009). CT-X antigen expression in human breast cancer. *Proc Natl AcadSci*, 106, 13493–13498.
  99. Rajagopalan K, Mooney SM, Parekh N, et al. (2011). A majority of the cancer/testis antigens are intrinsically disordered proteins. *J Cell Biochem*, 112, 3256–3267.
  100. Amir AL, van der Steen DM, van Loenen MM, Hagedoorn RS, de Boer R, Kester MD, et al. PRAME- specific Allo-HLA-restricted T cells with potent antitumor reactivity useful for therapeutic T-cell receptor gene transfer. *Clinical cancer research : an official journal of the American Association for Cancer Research* 2011;17(17):5615-25 doi 10.1158/1078-0432.CCR-11-1066.
  101. Wadelin F, Fulton J, McEwan PA, Spriggs KA, Emsley J, Heery DM. Leucine-rich repeat protein PRAME: expression, potential functions and clinical implications for leukaemia. *Molecular cancer* 2010;9:226doi 10.1186/1476-4598-9-226.
  102. Ikeda H, Lethe B, Lehmann F, van Baren N, Baurain JF, de Smet C, et al. Characterization

- of an antigen that is recognized on a melanoma showing partial HLA loss by CTL expressing an NK inhibitory receptor. *Immunity* 1997;6(2):199-208.
103. Epping MT, Wang L, Edel MJ, et al. The human tumor antigen PRAME is a dominant repressor of retinoic acid receptor signaling. *Cell* 2005;122:835–47.
104. Vulcani-Freitas TM, Saba-Silva N, Cappellano A, Cavalheiro S, Toledo SR. PRAME gene expression profile in medulloblastoma. *Arquivos de neuro-psiquiatria* 2011;69(1):9-12.
105. Boon K, Edwards JB, Siu IM, Olschner D, Eberhart CG, Marra MA, et al. Comparison of medulloblastoma and normal neural transcriptomes identifies a restricted set of activated genes. *Oncogene* 2003;22(48):7687-94 doi 10.1038/sj.onc.1207043.
106. Quintarelli C, Dotti G, De Angelis B, Hoyos V, Mims M, Luciano L, et al. Cytotoxic T lymphocytes directed to the preferentially expressed antigen of melanoma (PRAME) target chronic myeloid leukemia. *Blood* 2008;112(5):1876-85 doi 10.1182/blood-2008-04-150045.
107. Kessler JH, Beekman NJ, Bres-Vloemans SA, Verdijk P, van Veelen PA, Kloosterman-Joosten AM, et al. Efficient identification of novel HLA-A(\*)0201-presented cytotoxic T lymphocyte epitopes in the widely expressed tumor antigen PRAME by proteasome-mediated digestion analysis. *The Journal of experimental medicine* 2001;193(1):73-88.
108. Quintarelli C, Dotti G, Hasan ST, De Angelis B, Hoyos V, Errichiello S, et al. High-avidity cytotoxic T lymphocytes specific for a new PRAME-derived peptide can target leukemic and leukemic-precursor cells. *Blood* 2011;117(12):3353-62 doi 10.1182/blood-2010-08-300376.
109. Louis DN, Perry A, Burger P, Ellison DW, Reifenberger G, von Deimling A, et al. International Society Of Neuropathology--Haarlem consensus guidelines for nervous system tumor classification and grading. *Brain pathology* 2014;24(5):429-35 doi 10.1111/bpa.12171.
110. Louis DN, Perry A, Reifenberger G, von Deimling A, Figarella-Branger D, Cavenee WK, et al. The 2016 World Health Organization Classification of Tumors of the Central Nervous System: a summary. *Actaneuropathologica* 2016;131(6):803-20 doi 10.1007/s00401-016-1545-1.
111. Vera J, Savoldo B, Vigouroux S, Biagi E, Pule M, Rossig C, et al. T lymphocytes redirected against the kappa light chain of human immunoglobulin efficiently kill mature B lymphocyte-derived malignant cells. *Blood* 2006;108(12):3890-7 doi 10.1182/blood-2006-04-017061.
112. Quintarelli C, Vera JF, Savoldo B, Giordano Attianese GM, Pule M, Foster AE, et al. Co-expression of cytokine and suicide genes to enhance the activity and safety of tumor-specific cytotoxic T lymphocytes. *Blood* 2007;110(8):2793-802 doi 10.1182/blood-2007-02-072843.
113. Livak KJ, Schmittgen TD. Analysis of relative gene expression data using real-time quantitative PCR and the 2<sup>-</sup>(Delta Delta C(T)) Method. *Methods* 2001;25(4):402-8 doi

- 10.1006/meth.2001.1262.
114. Wilson KD, Stutz SJ, Ochoa LF, Valbuena GA, Cravens PD, Dineley KT, et al. Behavioural and neurological symptoms accompanied by cellular neuroinflammation in IL-10-deficient mice infected with *Plasmodium chabaudi*. *Malaria journal* 2016;15(1):428 doi 10.1186/s12936-016-1477-1.
115. Smits M, van Rijn S, Hulleman E, Biesmans D, van Vuurden DG, Kool M, et al. EZH2-regulated DAB2IP is a medulloblastoma tumor suppressor and a positive marker for survival. *Clinical cancer research : an official journal of the American Association for Cancer Research* 2012;18(15):4048-58 doi 10.1158/1078-0432.CCR-12-0399.
116. Grizzi F, Franceschini B, Hermonat PL, Liu Y, Chiriva-Internati M. Some remarks on the somatic expression of sperm protein 17. *International journal of cancer* 2004;111(6):972-3; author reply 4 doi 10.1002/ijc.20311
117. Di Stasi A, De Angelis B, Savoldo B. Gene therapy to improve migration of T cells to the tumor site. *Methods in molecular biology* 2010;651:103-18 doi 10.1007/978-1-60761-786-0\_7.
118. Infante P, Mori M, Alfonsi R, Ghirga F, Aiello F, Toscano S, et al. Gli1/DNA interaction is a druggable target for Hedgehog-dependent tumors. *The EMBO journal* 2015;34(2):200-17 doi 10.15252/embj.201489213.
119. Adoptive Immunotherapy Using PRAME-Specific T Cells in Medulloblastoma Domenico Orlando, Evelina Miele, Biagio De Angelis, Marika Guercio, Iolanda Boffa, Matilde Sinibaldi, Agnese Po, Ignazio Caruana, Luana Abballe, Andrea Carai, Simona Caruso, Antonio Camera, Annemarie Moseley, Renate S. Hagedoorn, Mirjam H.M. Heemskerk, Felice Giangaspero, Angela Mastronuzzi, Elisabetta Ferretti, Franco Locatelli, and Concetta Quintarelli. *Cancer Res.* 2018 Jun 15;78(12):3337-3349. doi: 10.1158/0008-5472.CAN-17-3140. Epub 2018 Apr 3
120. Hermes N, Kewitz S, Staeger MS. Preferentially Expressed Antigen in Melanoma (PRAME) and the PRAME Family of Leucine-Rich Repeat Proteins. *Current cancer drug targets* 2016;16(5):400-14.
121. Tajeddine N, Louis M, Vermylen C, Gala JL, Tombal B, Gailly P. Tumor associated antigen PRAME is a marker of favorable prognosis in childhood acute myeloid leukemia patients and modifies the expression of S100A4, Hsp 27, p21, IL-8 and IGFBP-2 *in vitro* and *in vivo*. *Leukemia & lymphoma* 2008;49(6):1123-31 doi 10.1080/10428190802035933.
122. Sun Z, Wu Z, Zhang F, Guo Q, Li L, Li K, et al. PRAME is critical for breast cancer growth and metastasis. *Gene* 2016;594(1):160-4 doi 10.1016/j.gene.2016.09.016.
123. Damm F, Heuser M, Morgan M, Wagner K, Gorlich K, Grosshennig A, et al. Integrative prognostic risk score in acute myeloid leukemia with normal karyotype. *Blood* 2011;117(17):4561-8 doi 10.1182/blood-2010-08-303479.



124. Szczepanski MJ, DeLeo AB, Luczak M, Molinska-Glura M, Misiak J, Szarzynska B, et al. PRAME expression in head and neck cancer correlates with markers of poor prognosis and might help in selecting candidates for retinoid chemoprevention in pre-malignant lesions. *Oral oncology* 2013;49(2):144-51 doi 10.1016/j.oraloncology.2012.08.005.
125. Szczepanski MJ, Whiteside TL. Elevated PRAME expression: what does this mean for treatment of head and neck squamous cell carcinoma? *Biomarkers in medicine* 2013;7(4):575-8 doi 10.2217/bmm.13.68
126. Iura K, Kohashi K, Hotokebuchi Y, Ishii T, Maekawa A, Yamada Y, et al. Cancer-testis antigens PRAME and NY-ESO-1 correlate with tumour grade and poor prognosis in myxoid liposarcoma. *The journal of pathology Clinical research* 2015;1(3):144-59 doi 10.1002/cjp2.16
127. Field MG, Decatur CL, Kurtenbach S, Gezgin G, van der Velden PA, Jager MJ, et al. PRAME as an Independent Biomarker for Metastasis in Uveal Melanoma. *Clinical cancer research: an official journal of the American Association for Cancer Research* 2016;22(5):1234-42 doi 10.1158/1078-0432.CCR-15-2071.
128. Tan P, Zou C, Yong B, Han J, Zhang L, Su Q, et al. Expression and prognostic relevance of PRAME in primary osteosarcoma. *Biochemical and biophysical research communications* 2012;419(4):801-8 doi 10.1016/j.bbrc.2012.02.110.
129. Zou C, Shen J, Tang Q, Yang Z, Yin J, Li Z, et al. Cancer-testis antigens expressed in osteosarcoma identified by gene microarray correlate with a poor patient prognosis. *Cancer* 2012;118(7):1845-55 doi 10.1002/cncr.26486.
130. Epping MT, Hart AA, Glas AM, Krijgsman O, Bernards R. PRAME expression and clinical outcome of breast cancer. *British journal of cancer* 2008;99(3):398-403 doi 10.1038/sj.bjc.6604494.
131. Oberthuer A, Hero B, Spitz R, Berthold F, Fischer M. The tumor-associated antigen PRAME is universally expressed in high-stage neuroblastoma and associated with poor outcome. *Clinical cancer research : an official journal of the American Association for Cancer Research* 2004;10(13):4307-13 doi 10.1158/1078-0432.CCR-03-0813.
132. Wong RWJ, Ngoc PCT, Leong WZ, Yam AWY, Zhang T, Asamitsu K, et al. Enhancer profiling identifies critical cancer genes and characterizes cell identity in adult T-cell leukemia. *Blood* 2017;130(21):2326-38 doi 10.1182/blood-2017-06-792184.
133. Steinbach D, Hermann J, Viehmann S, Zintl F, Gruhn B. Clinical implications of PRAME gene expression in childhood acute myeloid leukemia. *Cancer genetics and cytogenetics* 2002;133(2):118-23.
134. Rezvani K, Yong AS, Tawab A, Jafarpour B, Eniafe R, Mielke S, et al. Ex vivo characterization of polyclonal memory CD8+ T-cell responses to PRAME-specific peptides in patients with acute lymphoblastic leukemia and acute and chronic myeloid leukemia.

- Blood 2009;113(10):2245-55 doi 10.1182/blood-2008-03-144071.
135. Gutzmer R, Rivoltini L, Levchenko E, Testori A, Utikal J, Ascierto PA, et al. Safety and immunogenicity of the PRAME cancer immunotherapeutic in metastatic melanoma: results of a phase I dose escalation study. *ESMO open* 2016;1(4):e000068 doi 10.1136/esmoopen-2016-000068.
  136. Weber JS, Vogelzang NJ, Ernstoff MS, Goodman OB, Cranmer LD, Marshall JL, et al. A phase 1 study of a vaccine targeting preferentially expressed antigen in melanoma and prostate-specific membrane antigen in patients with advanced solid tumors. *Journal of immunotherapy* 2011;34(7):556-67 doi 10.1097/CJI.0b013e3182280db1.
  137. Pujol JL, De Pas T, Rittmeyer A, Vallieres E, Kubisa B, Levchenko E, et al. Safety and Immunogenicity of the PRAME Cancer Immunotherapeutic in Patients with Resected Non-Small Cell Lung Cancer: A Phase I Dose Escalation Study. *Journal of thoracic oncology : official publication of the International Association for the Study of Lung Cancer* 2016;11(12):2208-17 doi 10.1016/j.jtho.2016.08.120.
  138. Gonzalez-Galarza FF, Takeshita LY, Santos EJ, Kempson F, Maia MH, da Silva AL, et al. Allele frequency net 2015 update: new features for HLA epitopes, KIR and disease and HLA adverse drug reaction associations. *Nucleic acids research* 2015;43(Database issue):D784-8 doi 10.1093/nar/gku1166.
  139. Di Stasi A, Tey SK, Dotti G, Fujita Y, Kennedy-Nasser A, Martinez C, et al. Inducible apoptosis as a safety switch for adoptive cell therapy. *The New England journal of medicine* 2011;365(18):1673-83 doi 10.1056/NEJMoa1106152.
  140. Zhou X, Di Stasi A, Tey SK, Krance RA, Martinez C, Leung KS, et al. Long-term outcome after haploidentical stem cell transplant and infusion of T cells expressing the inducible caspase 9 safety transgene. *Blood* 2014;123(25):3895-905 doi 10.1182/blood-2014-01-551671.
  141. Zhou X, Dotti G, Krance RA, Martinez CA, Naik S, Kamble RT, et al. Inducible caspase-9 suicide gene controls adverse effects from alloplete T cells after haploidentical stem cell transplantation. *Blood* 2015;125(26):4103-13 doi 10.1182/blood-2015-02-628354.
  142. Zhou X, Naik S, Dakhova O, Dotti G, Heslop HE, Brenner MK. Serial Activation of the Inducible Caspase 9 Safety Switch After Human Stem Cell Transplantation. *Molecular therapy : the journal of the American Society of Gene Therapy* 2016;24(4):823-31 doi 10.1038/mt.2015.234.
  143. Parker BS, Rautela J, Hertzog PJ. Antitumour actions of interferons: implications for cancer therapy. *Nature reviews Cancer* 2016;16(3):131-44 doi 10.1038/nrc.2016.14.
  144. Parker BS, Rautela J, Hertzog PJ. Antitumour actions of interferons: implications for cancer therapy. *Nature reviews Cancer* 2016;16(3):131-44 doi 10.1038/nrc.2016.14.

